FABRICATION OF NICKEL(II) OXIDE (NiO) AND NICKEL(II) TITANATE ($NiTiO_3$) HETEROJUNCTION FOR VISIBLE LIGHT PHOTOCATALYSIS

by

Vullikanti Sai Aditya

A Thesis Submitted in Partial Fulfillment of the Requirements for the Degree of Master of Engineering in Nanotechnology

Examination Committee: Dr. Tanujjal Bora (Chairperson)
Dr. Ekbordin Winijkul
Dr. Bhawat Traipattanakul

Nationality: Indian
Previous Degree: Bachelor of Technology in Electronics and Communications Engineering
Jawaharlal Nehru Technological University
Hyderabad, Telangana, India

Scholarship Donor: AIT Fellowship

Asian Institute of Technology
School of Engineering and Technology
Thailand
July 2021

AUTHOR'S DECLARATION

I, Vullikanti Sai Aditya declare that the research work carried out for this thesis was in accordance with the regulations of the Asian Institute of Technology. The work presented in it are my own and has been generated by me as the result of my own original research, and if external sources were used, such sources have been cited. It is original and has not been submitted to any other institution to obtain another degree or qualification. This is a true copy of the thesis, including final revisions.

Date: 26th July 2021

Name (in printed letters): Vullikanti Sai Aditya

Signature:

ACKNOWLEDGMENTS

First of all, I would like to thank my advisor Dr. Tanujjal Bora, and Center of Excellence in Nanotechnology, AIT for giving me an amazing life changing opportunity to purse master's degree program in the field of nanotechnology. I am very thankful and blessed to have an amazing mentor, who has been guiding me, helping me in all the situations during my course of study at Asian Institute of Technology. The Center has helped to grow as a person and have been motivating me to use the knowledge to create solutions that have greater social impact and economic impact. This work is an example of our motivation to find solutions to most pressing challenges like environmental pollution.

I would like to thank my esteemed committee members Dr. Ekbordin Winijkul and Dr. Bhawat Traipattanakul for their valuable suggestions and directions during my research. I would also thank Prof. G. Louis Hornyak for being an amazing teacher, who have created a genuine interest in learning by doing. I would like to mention special thanks to Prof. Nitin Tripathi and office of the SDP for being an amazing guardian after our parents at AIT.

Finally, I would like to thank my parents, Dr. Vullikanti Chandra Sekhara Rao, and V. Uma Maheswari for facilitating and making this amazing opportunity to study at AIT and support me financially during my study period at AIT. This would not be possible without the AIT fellowship Program and JNTU Hyderabad.

I would like to mention a special thanks to my amazing friends Mr. Aujaswi Kumar Maurya, Ms. Lareesha Sai, Mr. Adithya Ganavaram, Mr. Sai Kiran Gaddamedi, Mr. Vivek Sharma Poudel, Syed Azhar who have been with me in all situations and making this AIT journey filled with a lot of lovely memories. I would like to thank all the fellow students from the Center of Excellence in Nanotechnology for helping and cooperating with me during the study.

ABSTRACT

In this study, we have successfully prepared a porous heterojunction photocatalytic coating composed of p-type Nickel (II) Oxide (NiO) and n-type Nickel (II) Titanate ($NiTiO_3$) and compared its visible light photocatalytic degradation of model organic dyes in water. We have used Methylene Blue, Methyl Red, Methyl Orange as our model pollutants. The porous NiO-$NiTiO_3$ heterojunction thin film, which offers enhanced surface area, was deposited on quartz substrate by using a combination of spray pyrolysis technique and modified Pechini technique. Scanning electron microscopy (SEM) and X-ray diffraction (XRD) techniques were used to investigate the morphological and crystalline properties of the NiO, $NiTiO_3$ thin films, and NiO/$NiTiO_3$ heterojunction. There were mixed phases of NiO, $NiTiO_3$, TiO_2 (Rutile) in the $NiTiO_3$ thin film was detected. Both NiO and $NiTiO_3$ thin films showed high crystallinity and good stability against humidity (RH ~80%) and light. UV-visible absorption spectrophotometer was used to study the optical properties of the thin film, and the heterojunction electrical behavior was evaluated by studying the current-voltage curves. Visible light photocatalytic degradation of model dyes in water was conducted using an artificial visible light source and dye degradation rates were evaluated to study the photocatalytic performances of the proposed thin films. Nearly 80% of methylene blue dye was degraded at the end of 150 minutes when illuminated with AM 1.5 spectrum. Methylene blue was the most degraded dye, while methyl orange being the least degraded one. The developed heterojunction photocatalyst showed promising photocatalytic activities and stability and has the potential for applications like textile industry wastewater treatment.

CONTENTS

LIST OF TABLES

LIST OF FIGURES

Figures **Page**

CHAPTER 1
INTRODUCTION

1.1 Background of the Study

In recent years, environmental pollution has become a global issue (Ge et al., 2016; Z. Jiang et al., 2016; Zhao et al., 2016) affecting our health and livelihood. One of the immediate effects of rapid globalization is an increase in pollutant substances in ground and surface waters resulting in serious health problems ((Z. Qu et al., 2017). So, there is an immediate need to innovate green and sustainable technologies that can help in controlling water pollution. Some of the recent nanotechnology-based approaches that have been proposed to tackle this problem are photocatalytic degradation, adsorption, and Fenton oxidation. (Barhoumi et al., 2016; Barrera et al., 2019)

Photocatalysis is a process where light energy is utilized by a nanostructured catalyst to accelerate one or more chemical reactions. When light is illuminated on the surface of a photocatalyst, excited electron/hole pairs are generated. Because of the activated state, the generated electrons and holes undergo chemical reduction and oxidation, producing reactive oxygen species (ROS) that can further catalyze chemical degradation of surface adsorbed pollutants. In a normal photocatalytic reaction, catalysts/substrates are triggered by light radiation, like ultraviolet/visible light of corresponding wavelengths, which is followed by electron-transfer to/from reactants that are acting in a redox reaction. In recent years, photocatalytic degradation has seen a significant growth mainly because of the use of clean and green energy sources to start the reactions, (i.e.) solar energy. (Chong et al., 2010).

There are a significant number of studies to optimize the performance of semiconductor photocatalysts for pollutant degradation which includes oxides, sulfides, nitrides, and oxynitrides. (Akpan & Hameed, 2009; Hara et al., 2003; Lei et al., 2003; Q. Li et al., 2015; Yu & Yu, 2008; Z. Zhang et al., 2010) There are many kinds of approaches used for enhancing the photocatalytic activity of the photocatalyst. One important way is to inducing defects, up conversion of lower wavelength light to higher, tweaking the morphology, etc. All the above listed methods are used to enhance the photo response of the material. While strategies like creating heterojunctions, plasmonic response, are used to create an efficient photocatalyst.

In this study, we have chosen a strategy of fabricating a heterojunction photocatalyst using two semiconductors (P-N) leading to a synergistic enhancement in the photocatalytic activity, by enhancing both the optical response and the photogenerated charge separation in the catalyst. For our study, we have used Nickel (II) Titanate ($NiTiO_3$) as an N-type semiconductor and Nickel (II) Oxide (NiO) as P-type semiconductor material. The two materials were used to synthesize a heterojunction photocatalyst that has improved optical response and charge separation upon visible light illumination. The heterojunction photocatalyst was then used to degrade organic dye pollutants in water and its performance was evaluated.

1.2 Statement of the Problem

In recent years there has been substantial interest in the scientific community to understand, analyze the reactions which happen when the materials are illuminated with the light. Most of the materials are semiconducting with bandgap energy between 1.1eV and 3.8eV. Some of the examples are semiconductor metal oxides, selenides, and sulfides. (Khan et al., 2015) In all the above-mentioned materials, the most effective photocatalytic materials are semiconducting metal oxides. Selenides and Sulfides are not stable due to the corrosive nature of the material, and most of them are toxic in nature. Whereas most semiconducting metal oxides are stable and not toxic when compared to selenides and sulfides.(Khan et al., 2015; Saravanan et al., 2013; Zhou et al., 2012) .

In all the metal oxide, Titanium Dioxide, TiO_2 (3.32 eV) is one of the best-known materials so far for achieving photocatalytic degradation of organic pollutants in water bodies. Many pieces of research show that TiO_2 has outstanding quantum efficiency and stability in an aqueous environment and is not toxic, which makes TiO_2 a good choice for use as a photocatalyst. (Inoue et al.,1979; Khan et al., 2015; Schneider et al., 2014) ZnO and CeO_2 are also used as photocatalytic materials because of their high adsorption properties and similar bandgap of 3.3 eV but both of these materials corrode in acidic medium(Choi et al., 2016; Fouad et al., 2006; Khan et al., 2014; Saravanan et al., 2013). However, ZnO and TiO_2 are highly active only in the UV region of the electromagnetic spectrum but have very low activity in the visible region due to their wide-bandgap.

Some of the key strategies that are used to improve the photocatalytic performance of the materials in the visible region are (1) doping of the material with another material to enhance the photo-absorption range of the material itself, (2) optimization of the active photocatalytic sites on the surface by making changes in morphology and lattice structure of the material, (3) inducing defects in the catalyst, (4) creating heterojunctions of the materials that have compatible bandgaps and can contribute to the effective charge carrier separation, hence enhancing the overall photocatalytic performance of the system on the whole.(B. Yang et al., 2019) Some of the key limitations in the first and the second strategies are having a controlled environment and sophisticated technology that is required to get a high-efficiency photocatalyst material, unavailability of scalable and low-cost synthesis techniques to get a high-efficiency photocatalyst. For the third strategy, controlling the defect density is a challenge and mostly not understood clearly. Due to these above-mentioned disadvantages, there has been a significant interest in the scientific community to develop heterojunction photocatalyst.

Some of the ideal characteristics of the eco-friendly efficient visible-light photocatalyst are the nontoxic nature of the material, high stability, efficient charge separation and transportation of the charge carriers, bandgap in visible light. Semiconductors have been long used in solar cells and paints which have suitable and tunable electronic and optical properties, but these materials are not widely used for photocatalytic coatings. We took some inspiration from the materials used for the fabrication of third-generation solar cells and paints. We have used NiO as a P-type semiconducting material (used as a hole transport layer in third-generation solar cells) and $NiTiO_3$ as an N-type semiconducting material (used frequently as a yellow dye/ pigmenting element in paints). NiO/$NiTiO_3$ P-N junction has a suitable heterojunction that has all of the properties mentioned above for an ideal visible light photocatalyst. The P-N junction formed has helped in inducing an internal electrical field that helped in better separation and transport of charge carriers. One of the key bottlenecks for this technology is the ability to fabricate these coatings using low-cost, and scalable fabrication techniques in all ambient atmospheres. In this study, therefore, we have focused on using simple wet chemical methods to fabricate the heterojunction photocatalyst.

1.3 Research Questions

1. How would the photocatalytic degradation efficiency of the material change when expanding the photo response (by forming thin-film-based heterojunction) of the photocatalytic coating?

2. Can we fabricate a visible light photocatalytic coating using a low-cost, reliable, stable, repeatable synthesis technique in all ambient atmosphere?

3. How will the photocatalytic degradation efficiency of the coating change when exposed to different light and humidity conditions?

1.4 Objectives of the Study

We aim to achieve the following objectives in this research.

1. Synthesis of photocatalytic thin films of (a) NiO, (b) $NiTiO_3$, and (c) $NiTiO_3$/NiO and compare their optical, electrical, morphological, and crystalline properties.
2. Study the stability of the heterojunction against different light and relative humidity conditions over a different interval of time.
3. Comparison of visible light photodegradation efficiency of all the above-fabricated coatings using different dyes (Methylene blue, Methyl Red, Methyl Orange) as model pollutants.

1.5 Scope of the Work

Our work is only limited to synthesis of heterojunction and characterization. We do not focus on enhancing the synthesis techniques, rather we have adopted them from the literature and used them with small changes in them. All the chemicals used during the synthesis process were declared by the vendors with their purity. We have used the analytical grade chemicals without any further purification. Our study is only limited to perform some initial stability tests only regarding the humidity and light exposure. Our study is limited to test the stability in terms of electrical and optical response only. Our study is limited to study the stability in the laboratory environment only. No tests were conducted in field. All the results produced using the third-party equipment are not calibrated, or used by the researcher, rather was handled by a professional from the testing centers. All the photocatalytic degradation tests were only performed using a constant source of artificial illumination with a fixed intensity of light.

1.6 Organization of the Study

In Chapter 1 we introduce the background and the rationale of the study with an overview of the objectives of this study. In Chapter 2 we give a detailed review of the photocatalytic process, coatings, material properties, and different fabrication procedures that currently are used. In Chapter 3 we have discussed in detail the methodology along with the conditions that were used while doing the experimentation in the lab. We also discuss methods that were used to conclude the results. In Chapter 4 we explain the results obtained from the experimentation. In the discussion section, we discuss the results and respective analysis of the results. Finally, in Chapter 5 we conclude the study based on our results and provided recommendations for future studies.

CHAPTER 2
LITERATURE REVIEW

2.1 Introduction

Every day, huge volumes of waste material are dumped in the environment that we live in, as pollutants. Organic pollutants have the biggest share among all the pollutants. Organic pollutants are mainly generated due to extensive industrial, farming, and domestic applications. These pollutants enter the natural resources, air, water streams, and soil. These contaminants create irreversible damage to our environment. (Chaturvedi & Verma, 2015; Cooper, 1993; Davidson et al., 2003; Pimentel D, McLaughlin L, Zepp A, et al. Environmental and Economic Effects of Reducing Pesticide Use. BioSci. 1991;41(6):402–409.; Robinson et al., 2001; Zhao et al., 2016). The organic contaminants, released in the gaseous phase, go into the air, and ultimately, they get absorbed into natural resources like soil, water, and vegetation due to rain or through the process of condensation. (Wania & MacKay, 1996) .

Pollutants then can enter human beings through different processes like inhalation of air, through food and drinks, resulting in havoc in multiple organs of the human body like digestive, respiratory, urinary, cardiovascular, and nervous systems (ElSalam, 2013; Kampa & Castanas, 2008; Reid et al., 1973). Huge research groups have been focusing their work on devising innovative and eco-friendly processes to eliminate organic pollutants from the environment through different approaches, i.e., physical, biological, and chemical methods. Organic contaminants are present in the vicinity of wastewater treatment units, oil, and chemical industries, ultimately mix into the natural resources in the environment through known or unknown means. Some organic contaminants can cause a wide range of sicknesses which include headache, fatigue, nasal irritations, acute breathing problems. Other organic contaminants are carcinogenic or can cause liver/ organ failure. (OEHHA. California Office of Environmental Health Hazard Assessment. 2007) Currently, uncontrolled air pollution and water pollution have increased health issues and cost billions of dollars to clean the environment.

Organic pollutants are detected through smell (odor) when present in higher concentrations in the environment, but at lesser concentrations, we need advanced

techniques like atomic absorption spectroscopy, gas chromatography, and optical spectroscopy (UV fluorescence, visible, and FTIR) techniques. Most of today's techniques of purification have significant drawbacks in the terms of speed, greater cost. So, there has been a significant emphasis that has been granted to clean air and water using nanoengineered photocatalytic materials, which have an immense potential to break the organic pollutants to carbon dioxide (CO_2) and water with no harmful byproducts.

2.2 Photocatalysis

Photocatalysis is a process in which the catalyst receives electromagnetic radiation (such as visible light) and gets into the excited state due to the excitation of electrons from the material. Then this exciting photocatalyst undergoes an intersystem crossing from the starting material and returning to its ground state without any change in the material. The excited state photocatalytic material will undergo redox reactions. In short, Photocatalysis is the speeding up of photoreaction in presence of a catalyst. A photocatalyst can be described as a material that absorbs light, producing charge carriers that can enable chemical reactions between participants and regenerate/retain their chemical composition after every cycle of chemical reactions. (Khan et al., 2015)

Nano photocatalysts refer to any material that has the above properties of photocatalysts and the size of these catalysts below 100 nanometers in any dimension. All Nanomaterials have very high surface-to-volume ratios, which increases the total number of active sites on the catalyst surface. (P. Zhang et al., 2016) .Photocatalysis varies in detail in terms of types of reactions and corresponding mechanisms, can be characterized by four important steps:

(I) Absorption of light resulting in the generation of charge carriers
(II) Splitting of charge carriers
(III) Transfer of charge carriers to the surface of photocatalysts
(IV) Consumption of the charge carriers on the surface of the photocatalyst through oxidation-reduction reactions.

Figure 2.1

Photocatalyst Mechanism

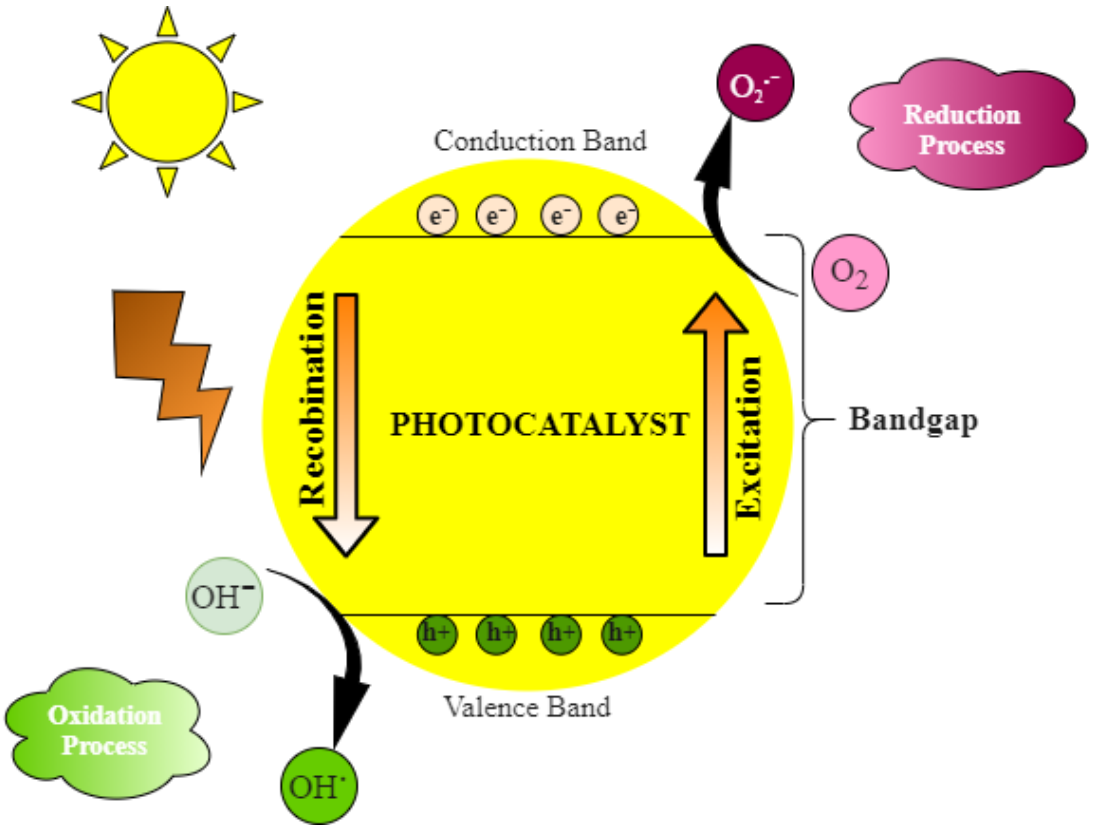

Oxidation Mechanism

The photocatalyst's surface meets moisture/water and gets absorbed on the surface of the photocatalyst. When water gets oxidized due to holes generated in the valence band of the material because of the shifting of electrons to the conduction band of material, when the material is irradiated with visible light, finally making a path for the generation of hydroxyl radicals. Generally, these agents have strong oxidation power. Thereafter, hydroxyl radicals will result in a reaction with organic matter (like dyes). In the presence of oxygen, if the above process happens, organic compounds will undergo radical chain reactions. In this case, as mentioned above, the organic matter ultimately mineralizes to be converted into carbon dioxide and water. As mentioned in the above circumstance, organic compounds would react directly with holes, finally which leads to overall decomposition.

Figure 2.2

Oxidation Mechanism

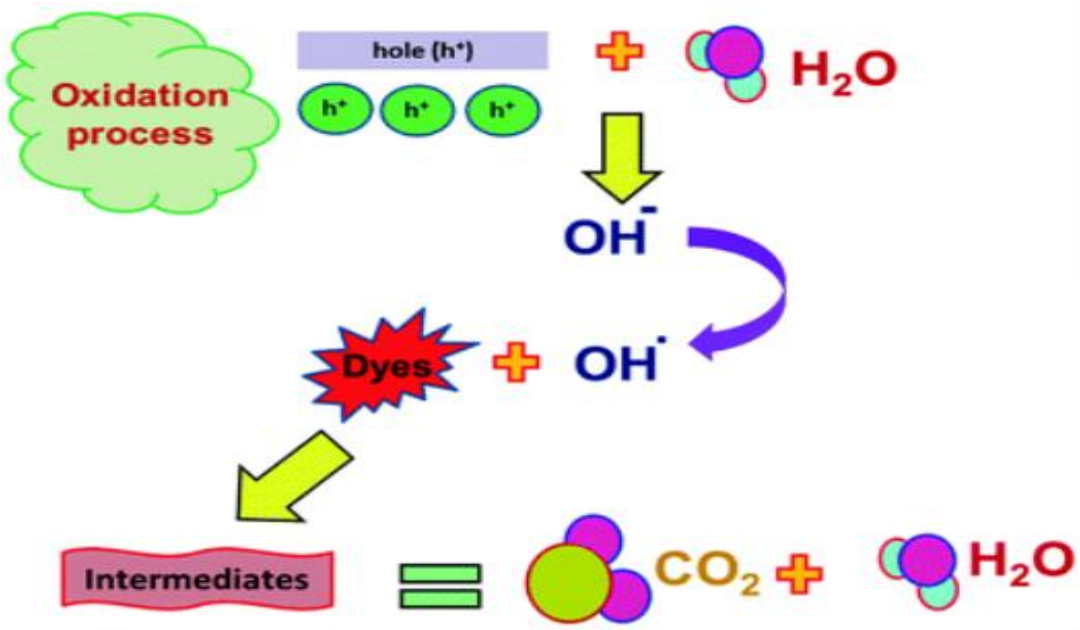

Reduction Mechanism

The reduction of atmospheric oxygen into superoxide occurs as a pairing reaction. Oxygen Reduction happens as an alternative to the generation of hydrogen because oxygen gets reduced very easily. Electrons present in the conduction band of the catalyst react with dissolved oxygen in the water to form anions called superoxide anions. Superoxide anions react with intermediate species in the oxidation reaction, ultimately producing peroxide ions followed to form water. This Reduction happens in organic matter when compared to water. So, the increased concentration of organic matter tends to increase the total number of holes. This helps in reducing the charge carrier recombination and results in the enhancement of photocatalytic activity.

Figure 2.3

Reduction Mechanism

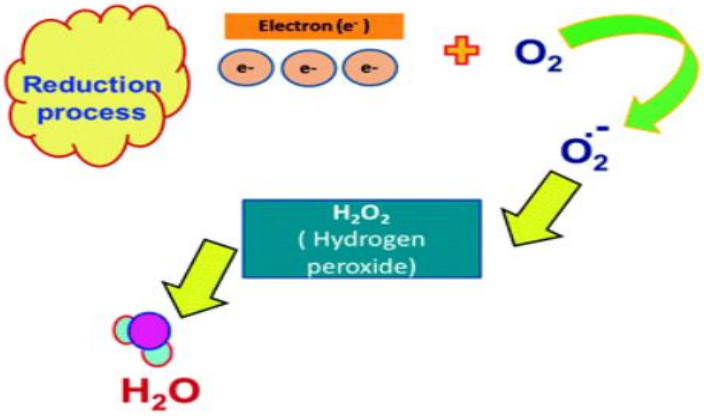

2.2.1 History of Photocatalysis

In early 1901, chemist Giacomo Ciamician conducted some of the first experiments to check whether light alone could drive any chemical reactions(Albini et al., 2008.) He performed experiments in the presence of red and blue lights. He discovered that a chemical reaction happened only in blue light. He designed experiments such that it excluded the likelihood that reactions were instead driven by thermal heating produced because of light. It was only in 1911, "photocatalysis" keyword was first mentioned in some of the scientific literature. (Bruner & Kozak, 1911) The scientific community referred to the bleaching of Prussian blue in the presence of Zinc Oxide (ZnO) in the illumination as photocatalysis. This has inspired the scientific community for performing consequent experiments using Zinc Oxide as a photocatalytic material in new chemical reactions like a reduction of Ag^{+} to Ag in the illumination of visible light in 1924(Baur et al., n.d.) Later in the year 1932 in the reduction reaction of $AuCl_3$ to Au and $AgNO_3$ to Ag was conducted out in the presence of Nb_2O_5 and TiO_2 as photocatalytic materials. Later, in 1938 TiO_2 was tested as a photosensitizer that can be used to bleach dyes along with the presence of O_2 in the environment. (Goodeve & Kitchener, 1938)Till the late 1960's Photocatalysis could not change the interest of the scientific community as it did not have any mainstream applications. In the early 1970's the first-ever oil crisis and concerns to find an eco-friendly alternative to fossil fuels changed has brought photocatalysis as one of the interesting technologies that could be an alternative to the existing fossil fuel technologies. (Zhu & Wang, 2017) In the year 1968, scientists at the Bell Lab created O_2 in a lab environment on the surface of TiO_2. (Boddy, 1968) In the year 1972, photo-assisted H_2O oxidation along with the

production of H_2 was achieved using electrodes made of TiO_2 illuminated with UV radiation, which was reported by Fujishima and Honda. (Fujishima et al., n.d.) In the year 1977 for the first time, water splitting (through the photocatalytic process) was achieved with no external energy other than light, resulting in a yield of O_2 and H_2 in presence of argon gas. Later in 1979, photocatalytic CO_2 reduction was reported using different inorganic semiconductors by Fujishima and his research group. (Inoue et al., 1979)These efforts have led to the advances in applications of photocatalysis for many new fields, that drew significant interest in the scientific community in the early 1980s to research analogous reactions using TiO_2 as the photocatalytic material. Since the 1980s, investigations were concentrated on recognizing the underlying principles, improvising the efficiencies of the photocatalytic performance, exploring new photocatalytic material, and developing the scope of the reactions. For example, the super-hydrophilicity effect due to the photocatalytic activity was discovered on TiO_2 in 1997. (Blondeel et al., 1983.; Halmann et al., 1984.)

2.2.2 Understanding Heterogeneous Photocatalysis

In any semiconductor, we can use a couple of quantities to define the semiconducting properties of materials; they are carrier mobility and carrier density. Where carrier mobility can tell us how good the material is in transporting the mobile charge carriers in the material. Whereas carrier density refers to the number of carrier charges that can be packed in each amount of volume of the semiconducting material. These two quantities are inversely proportional. We can observe these properties in materials such as graphene and III-V group (GaN, InP) semiconductors have high mobility of the carriers in the material and very low carrier density because the band structure of these materials are inherently built in such a way that they can only hold a very small amount of charge carriers but they can move the charges in an extremely efficient manner. On the other hand, some materials have high carrier densities and low carrier mobilities such as Transition metal oxides ($NiTiO_3$). Many materials such as graphene and III-V semiconductors tend to have conduction happening through the valence bands that have prominent characteristics of s and p orbitals. These materials have very high carrier mobilities because of the high dispersive nature of the s-p hybridized orbitals. While in the case of transition metal systems we tend to see d band conduction where the carrier density goes up but the carrier mobilities in these systems are extremely low but the carrier density is extremely high. There has been a significant effort being made by the

scientific community to take these systems and retain the carrier density and increase carrier mobility. Two major factors that affect carrier mobility are 1.the large density of states in the system and 2.the scattering processes that happen in the system.

Let us take a semiconducting material that has some of the empty energy levels and gradually when we move down, we have a gap in the empty energy levels. The gap in the energy levels can be described as the difference between the highest energy level of the valence band and the lowest energy level of the conduction band. Then we have a set of energy levels that are gradually filled with electrons (i.e) filling the bonding orbitals with electrons there are electrons in each bonding orbitals and these electrons are known as valence electrons and the energy band that has electrons are known as the valence band. The gap plays an important role in defining the absorption of the photons of suitable energy. The energy bandgap in the semiconductor can be fine-tuned to energy levels that determine the part of the solar spectrum that is absorbed (i.e) visible region, UV, or near IR regions of the solar spectrum. The empty orbitals are described as the molecular conduction band. These are also called antibonding orbitals as the energy level is much higher when compared to the energy of the bonding orbitals. When this semiconducting material is hit with a photon of suitable energy then the electron from the bonding orbital is excited to one of the lowest empty antibonding orbitals, which essentially creates a vacancy in the bonding orbital, in many cases, this is referred to as a hole. Generally, the hole is considered an arbitrary positive charge that is generated when an electron is excited.

To make an efficient heterojunction photocatalyst we sandwich this semiconducting material with suitable materials, such that we will be successfully withdrawing a hole from one side of the active material. The gradient of energy levels across the different materials creates an electrical field that behaves as a guiding force in the transfer of the charges from one material to another. The selection of the complementing materials is done in a particular way that the generated hole from the semiconducting material is readily transferred to the electrode material this material is responsible for grabbing the hole that is generated from the conduction band to the valence band with the least amount of energy lost during the process. On the other side of the active photocatalyst material, there is a redox reaction that happens in presence of atmospheric moisture or

water which takes the electron from the surface and turns the water into redox radicals like super ion or hydroxyl ions. These redox ions react with organic dyes and other pollutants present in the atmosphere/environment to reduce them into less harmful substances.

2.3 Visible Light Photocatalysts

Figure 2.4

Electromagnetic Spectrum

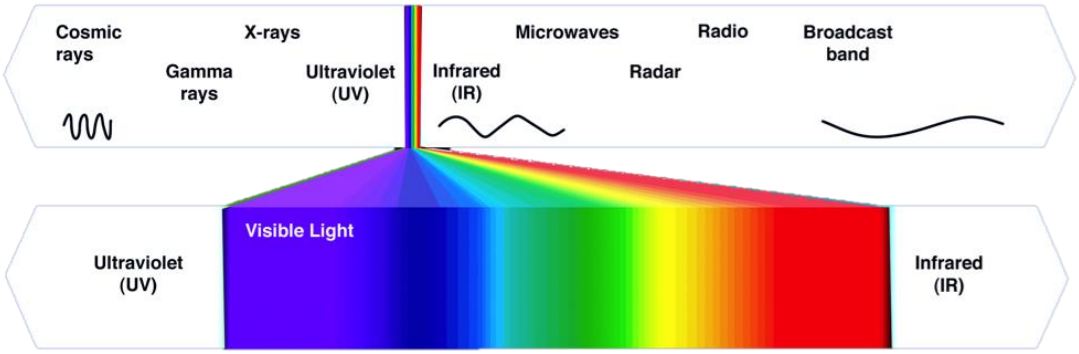

Visible light photocatalysis refers to a phenomenon where an active photocatalytic material absorbs the light in the range of the visible electromagnetic spectrum and gets to an excited state resulting in the generation and driving of the reaction using photogenerated charge carriers. Visible photocatalysis is used in many areas like detoxification of water, treatment of air pollutants, generation of antimicrobial coatings, etc. One of the important advantages of using visible light as a source is that it is abundantly available in nature, safe for human beings, and a completely eco-friendly source of energy. (Gunti et al., 2018). Visible Photocatalyst can be divided broadly into two types: single material photocatalysts or heterojunctions (which include Z-scheme systems).

Figure 2.5

Different Types of Photocatalysts (I)N-Type Photocatalyst ;(II) P-Type Photocatalyst ;(III) Heterojunction Photocatalyst

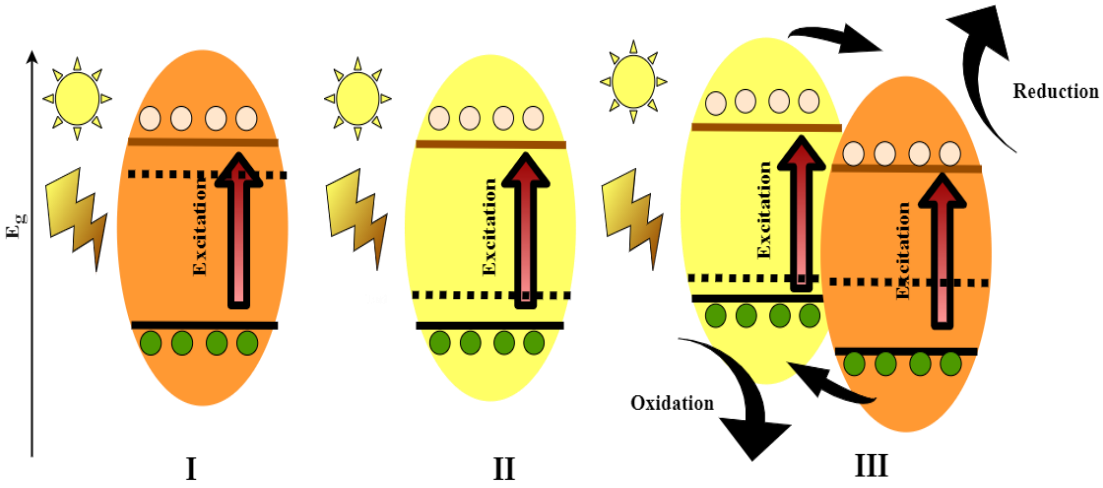

2.3.1 Single Material Photocatalysts

Single material photocatalysts are generally a semiconductor of a specific type (i.e. *n*-type and *p*-type semiconductors). The bandgap in the material is within the scope of the visible spectrum. In the case of p-type photocatalysts, the fermi level is closer to the valence band of the material and facilitates the transfer of holes as majority charge carriers. Whereas in n-type photocatalysts the Fermi level is closer to the conduction band of the semiconductors and enables the transfer of electrons as majority charge carriers. Some of the main drawbacks in single material photocatalysts are simultaneously achieving, favorable band alignments in the electronic structure and narrow bandgap, and low recombination of charge carriers in a single material. Some of the strategies that are used for enhancing the performance of visible-light single-material photocatalysts can be used to enhance the performance of individual materials in sophisticated photocatalysts. Some of the main strategies involve the optimization in surface area, crystal structure, and morphology; the organization and control of native defects; or doping the materials with different materials to finetune the optical and electronic properties. Some of the material can also be used as sensitizers which are used to optimize the absorption of materials in the visible spectrum of the electromagnetic spectrum.

2.3.2 Heterojunction Photocatalysts

To increase absorption of the light in the visible region, without compromising with the increase in the recombination rate of charge carriers, semiconductor–semiconductor or metal-semiconductor heterojunction photocatalysts can be used. Heterojunction photocatalysts are broadly classified into 3 types:

1.Common heterojunction photocatalysts

2.Z scheme heterojunction photocatalysts

3.Plasmonic heterojunction photocatalysts

Common Heterojunction Photocatalysts

One type of the major type of classification is based upon the energy band configuration namely the Stradling gap (Type I); Staggered gap (Type II); Broken Gap (Type III).

Figure 2.6

Various Mechanisms in Heterojunction Photocatalysts (I)Stradling Gap;(II) Staggered Gap ;(III) Broken Gap

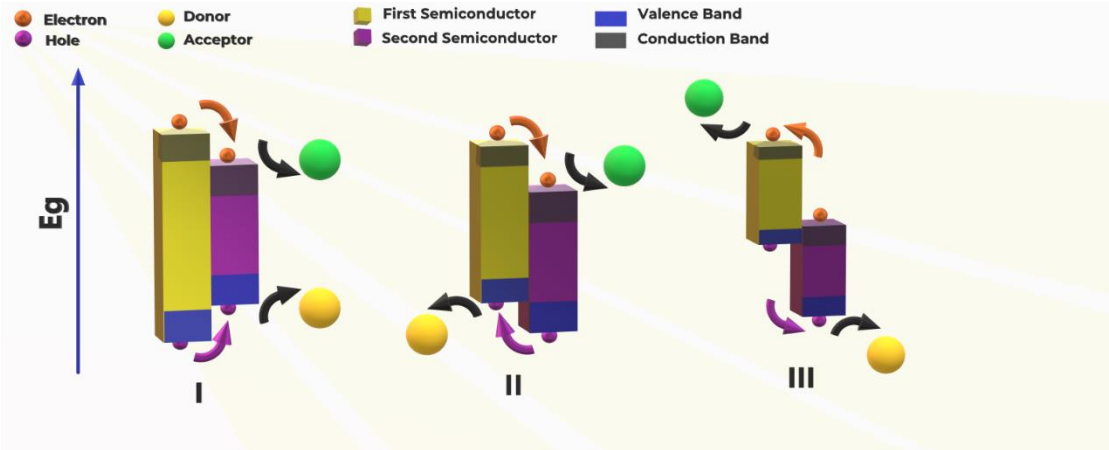

In the Stradling gap type of heterojunction semiconductor, the valance band of the first semiconductor is lesser than the valance band of the second semiconducting/ conducting material. The conduction band edge of the second material is lesser than the conduction band of the first semiconducting material. When these types of photocatalysts are irradiated with light charge carriers will be collected at the valence band and the conduction band levels of the second semiconducting material, respectively. In this type of photocatalyst, the charge carriers are accumulated on the

second semiconductor material only, the charge carriers cannot be efficiently separated for the Stradling gap type heterojunction photocatalyst. (Zhou et al., 2012)

For the Staggered gap (Type II) heterojunction photocatalyst the valence band and the conduction band levels of the first semiconducting material are higher than the corresponding photocatalyst the conduction band and the valence band levels of the second semiconductor. Therefore, the electrons that are generated when illuminated with light will flow to the second semiconducting material, while holes will migrate to the first semiconducting material under light illumination, thus resulting in efficient spatial separation of charge carriers in two different materials and at different energy levels. Like the type-I heterojunction, the reaction potential of the Staggered gap (Type II) heterojunction photocatalyst is decreased due to redox reaction happening on second semiconducting material with a lower reduction potential and primary semiconducting material with lower oxidation potential. (Marschall, 2014; Moniz et al., n.d.; H. Wang, Zhang, et al., n.d.)

The architecture of the Broken Gap (Type III) heterojunction photocatalysts is analogous to that of Staggered gap (Type II) heterojunction photocatalysts with the exception that the staggering gap between the two semiconducting materials becomes extremely high that the bandgaps of the materials do not overlap at all. Thus, the charge carriers transfer between the two semiconducting materials will not occur at the heterojunction. This makes this type of photocatalyst unsuitable for improving the separation of charge carriers. (Hyun et al., 2013; Shi & Chopra, 2013)

Z scheme Heterojunction Photocatalysts

In a Z-scheme photocatalyst, the electron transfer happens from the conduction band of one semiconducting/conducting material into the valence band (VB) of another material via an electron mediator that confirms there is a higher difference between reduction and oxidation energy levels when compared to the heterojunction(Huang et al., 2019; L. Jiang et al., 2018) These types of hetero photocatalysts can theoretical maximum efficiency of 40% in terms of conversion efficiency of solar energy, which is comparatively greater than the conversion efficiency of single photocatalysts(around 30%). (Y. Wang et al., 2018)

Plasmonic Photocatalysts

For all the above-listed photocatalyst classes of materials, we can improve photocatalytic activity by combining metal nanoparticles to use plasmonic effects that happen in metal nanoparticles, i.e. resonant oscillations of electrons that are present within the metal nanoparticle. The wavelength (of Plasmonic oscillations) of material directly depends on the dielectric function of the material, morphology, and size. (Q. Jiang et al., 2018). When these Plasmonic effects are combined with other functions for the material we get enhanced photocatalytic performance. One example is the inclusion of plasmonic nanoparticles in Z-scheme photocatalysts. (Lu et al., 2017) The enhancement of the photocatalytic activity due to the inclusion of plasmonic nanoparticles may occur in multiple mechanisms, namely, plasmon resonance energy transfer, injection of the hot electron, enhancement of localized electromagnetic field, also from dipole-dipole interaction of the materials. ("Evidence for Plasmonic Hot-Electron Injection Induced Superior Visible Light Photocatalysis by G-C3N4 Nanosheets Decorated with Ag–TiO_2 (B) and Au–TiO_2.One of the most common plasmonic nanoparticles is Ag (Silver) nanoparticles because of their strong nature of localized surface plasmonic resonance even though other metals are also used for plasmonic enhancement. (Kumar Ray et al., 2019)

2.4 Strategies Employed to Enhance the Efficiency of Photocatalysts.

The first method of enhancing the performance of photocatalysts is to enhance their photocatalytic activity by controlling the structural orientation of the crystals/ exposing the more reactive planes of the crystal. The crystal/lattice structure of a semiconducting material alters the photocatalytic efficiency of the material. (Xie et al., 2015). Generally, photocatalytic reactions happen on the active sites of a photocatalyst's surface, and photocatalytic efficiency can be improved by reducing the size to nanometers and optimizing the surface morphology of the material. (Ge et al., 2016) The overall number of active sites increases with an increase in the specific surface area of the material which in return increases in the crystal facets that have higher photocatalytic activity. (Ge et al., 2016; Kumar et al., n.d.) Typically, effects of change in morphology of the material (for example, nanocrystals vs nanowires of the same material) on overall photocatalytic activity of the material is interpreted as structural sensitivity of the nanostructure. (Kumar et al., n.d.)

The second method is to control the electronic band structure of the existing photocatalysts materials through modification of the defect modification or doping of the material with ions. Doping is one of the most common methods to spread the absorption response of a material to longer wavelengths of the electromagnetic spectrum. It is also used to control the growth of photocatalyst to alleviate additional reactive surfaces to enhance overall photocatalytic activity. (Ruan et al., 2019)One example of this approach is the modification of TiO_2, doping of TiO_2 with Nitrogen, which is reported with exceptional photocatalytic properties in the illumination of visible light(Asahi et al., 2001; Hara et al., 2003)

The third method is creating heterojunctions with different semiconductors having distinct band structures, in a particular way that generation and splitting of photogenerated carriers are understood by matching of electronic bandgap structures of the materials. Some of the examples that have demonstrated the success of this approach are AgI/BiOI, Bi_2O_3/$BiWO_6$, and TiO_2/WO_3 heterojunctions that could efficiently inhibit charge carrier recombination and significantly improved photocatalytic performance. (Peng et al., 2014; Puddu et al., 2007; Q. Yang et al., 2017)

Based on the success of all the above-mentioned three approaches, through this study, we plan to fabricate heterostructure leading to the enhancement of photocatalytic coating efficiency by improving the optical response of the semiconductors and limiting the recombination of photogenerated charge carriers within the material. We choose nickel titanate ($NiTiO_3$) and nickel oxide (NiO) as two semiconducting materials for our heterostructure nano-photo catalytic coating.

2.5 Nickel Titanate

Figure 2.7

Ilmenite Structure Lattice (I)Top View;(II) Three-Dimensional View ;(III) Side View.

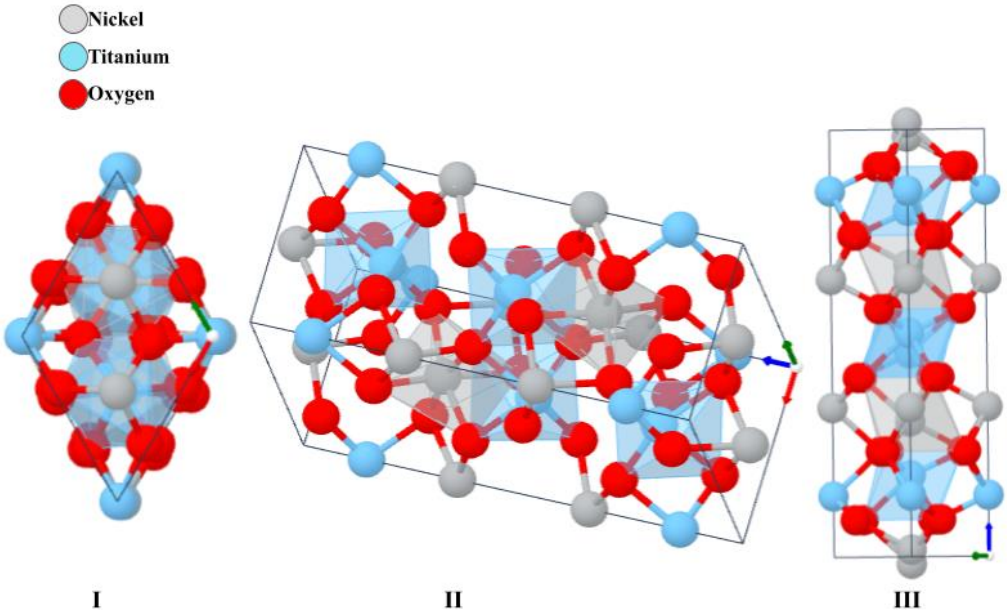

Metal Titanate oxides include metals, like cobalt, nickel, ferrite, copper, zinc, lead are well-identified universally as inorganic functional materials that have a broad range of applications in various industries. Some of the industrial uses are the raw material in the manufacturing of rectifiers, electrode plates of a solid oxide fuel cell, hydro carbonate catalyzers, gas sensing devices, color mixtures, etc.(Fisch, 1995; Harris et al., 1997; Phani & Santucci, 2001; Taguchi et al., 1992)

$NiTiO_3$ has an ilmenite structure lattice. Ti & Ni atoms preferably have octahedral coordination along with alternating layers of cations that are filled only by Ni^{2+}& Ti^{4+}only. (Inceesungvorn et al., 2014; Lin et al., 2006a; Nguyen-Phan et al., 2013) $NiTiO_3$ is an n-type semiconductor and has a bandgap of 2.15 eV. (Fan et al., 2012) $NiTiO_3$ is one of the promising materials that could be used for visible light-photocatalysis because of its narrow bandgap, where charge carriers can be easily excited to the conduction band by illuminating the material with visible light. It also has some weaknesses like poor quantum efficiency and a rapid recombination rate of charge carriers when it is used as a photocatalyst with individual phases. Electron transitions from Oxygen(O_2) / Titanium (Ti^{4+}) (conduction band) happens in presence

of UV light. When illuminated with visible light, Nickel (Ni^{2+})/ Titanium (Ti^{4+}) transitions happen. But because of the geometry of $NiTiO_3$, weakens the strength of the oscillation's leading to the Ni^{2+} / Ti^{4+} weak charge transfer. $NiTiO_3$ has a great blend of 3d orbital of Ni along with 2p orbital of O in the valence band. There is a pseudo bandgap of nearly 0.3 eV that is created in the valence band of $NiTiO_3$ approximately at 1.4 eV is a result combination of orbitals because of the strong covalent nature of Ni–O bonds.

To overcome the fast recombination, there have been multiple studies to change some of the properties of $NiTiO_3$ which include the making of composite materials by making use of carbon-based materials like gC3N4(Pham, Kang, et al., n.d.; Pham, Nguyen-Huy, et al., n.d.; Sadjadi et al., 2008; H. Wang, Yuan, et al., n.d.), making use of heterojunctions made along with inorganic nanoparticles (Inceesungvorn et al., 2014), and as well as the doping into the crystal structure. (Lenin et al., n.d.; Lin et al., 2006b; Pham, Kang, et al., n.d.). We will be using the strategy of heterojunction photocatalysts to overcome this problem of rapid recombination.

2.6 Nickel Oxide

NiO has a wide bandgap. Currently, transparent conducting metal oxide (TCOs) thin films, like tin oxide, indium oxide, and zinc oxide, are usually utilized as materials for coatings on glass surfaces for optoelectronic devices and transparent electrodes. (Gopchandran et al., 1997; Joseph et al., 1999) All of the above-mentioned thin-film materials are *n*-type semiconducting materials. There has been growing interest in *p*-type semiconducting films with an increasing need for in which hole injection is required like optical windows for devices. Nickel Oxide is a *p*-type semiconductor material and has a bandgap in a range of 3.6 eV - 4.0 eV. Nickel Oxide is transparent to a wide range of electromagnetic spectrum which makes NiO a material that can address a wide range of the need for such kind of material. A widely used application of NiO is as P-type oxide material for MOS devices(Sasi et al., n.d.) Structurally NiO has a cubic lattice structure, similar to NaCl where Ni^{+2} and O^{2-} occupy the octahedral lattice sites.

On the other hand, one of the interesting applications of NiO is in third-generation solar cells. NiO has gained immense interest in the scientific community as a hole transport material in the perovskite solar cells due to its optoelectronic properties. It has been proven that the use of NiO increases photoconversion efficiency.

Typically, NiO in its Pure stoichiometric form is an excellent electrical insulator at room temperature. Nevertheless, oxygen is present in excess in practice, because of the presence of Ni_2O_3 and NiOOH. Generally, NiO always tends to exist in a nonstoichiometric state, which is broadly denoted as NiOx. Due to the existence of extra oxygen usually ends with vacancies of Ni (i.e.) holes, so NiOx is usually behaving as p-type semiconducting material. NiOx has a work function of 5.4 eV. NiO has wide bandgaps which range from 3.6to 4.0 eV, this bandgap enables its high transparency mainly in the UV and visible spectrum. Thus, making NiOx a potential p-type transparent conductive oxide. (Sato et al., 1993; Sawatzky & Allen, 1984)

2.7 The Architecture of the Heterogeneous Photocatalytic Coating

One of the key steps is the generation of charge carriers at the $NiTiO_3$ surface. Separation and movement of the charges will be promoted due to the electronic band displacement at the NiO/$NiTiO_3$ junction. The above-mentioned separation facilitates the effective use of the photogenerated charge carriers. When these coatings are illuminated with UV and Visible spectrum, electrons would absorb energy in $NiTiO_3$ and NiO, then they would get excited from the valence band of the respective material to the conduction band, leaving behind holes that are generated at the valence band. Near the heterojunction interface at $NiTiO_3$ and NiO, the NiO conduction band (−1.23 eV ($E_{NHE}V$)) (Rawool et al., 2018) comparatively lower when compared to that of $NiTiO_3$ (0.23 eV ($E_{NHE}V$)) (S. Li et al., 2018), essentially resulting in the free flow of electrons from the conduction band of NiO to $NiTiO_3$. Simultaneously, Organic dye will be decomposed because of the holes that are generated in both NiO and $NiTiO_3$ when illuminated with light. However, the valence band edge of $NiTiO_3$ is greater when compared to the reduction potential of H_2O i.e. (2.38 eV). The superoxide (O^{2-}) radicals and holes are going to play a very important role to play in the process of photocatalytic degradation due to NiO/$NiTiO_3$ heterojunction. One more thing that would play a crucial role is the differences between the valence band potentials of $NiTiO_3$ and NiO. This difference drives the holes generated at $NiTiO_3$ to the valence band of NiO.

Additionally, the p-n heterojunction created by NiO and $NiTiO_3$ results in the formation of a localized electric field at the interfaces. The charge carrier movement in different directions which is driven by the localized electric field will effectively help us in suppressing the recombination, thereby essentially boosting the photocatalytic efficiency of the photocatalytic coating.

CHAPTER 3
METHODOLOGY

3.1 Materials & Equipment

Following chemicals and materials were used in this study:

Titanium (IV) Isopropoxide (98% purity from Alfa Aesar), Nickel (II) Acetate tetrahydrate (98% purity from Aldrich), Hydrochloric acid (HCl), Deionized water (18.2Ω) (from AKA smart2 pure D.I water dispenser), Quartz substrate, Acetone, Ethanol (RCI Labscan), Methylene Blue (Carlo ERBA), Methyl Red (Carlo ERBA), Methyl Orange (Carlo ERBA). Only chemicals of the analytical grade were used directly without any further purification.

Following equipment were used in the study: USB 4000 with DH2000, Keithley 617 Electrometer, NI GPIB -USB-HS connector, A system with software (Python3.9.5, NI-VISA drivers, Spectra suite), Ultrasonicator (Kudos SK 3210HP), Airbrush with portable air compressor, Deerma FH630 ultrasonic humidifier, Sensitive balance (Sartorius CP2250), Hotplate (IKAC-Mag HS7), beakers, measuring cylinders.

3.2 Substrate Preparation

We have used FTO coated glass (85% transparency in the visible region) and Quartz glass as our substrates. The FTO coated glass was used for samples to perform electrical characterization. All substrates (FTO, Quartz) were cut into 20 x 20 mm. The substrates were then thoroughly washed using a detergent and water mixture and ultrasonicated for 20 mins in DI Water. Samples were rinsed with DI water 2 times. All the substrates were again cleaned for 2 cycles, using Acetone, Ethanol, and DI water using ultrasonication for 15 mins. Subsequently, substrates were cleaned using tissues and placed in a clean tray with aluminum foil and heated to 230℃ using a convection oven and kept for 20 mins. The substrates were allowed to be cooled down to room temperature.

3.3 Synthesis of NiO Thin Films

We used a bottom-up approach for the synthesis of NiO thin films using a spray pyrolysis technique. The main properties that determined the quality of the thin films were substrate type, the temperature of the substrate, spray rates, and droplet sizes

which depend on spray rate, carrier gas, the diameter of the nozzle, and concentration of pressure of the carrier gas. (Manifacier et al., 1981; Sakhare et al., 2016) From the above, the spray pyrolysis technique is highly tunable and controllable in nature. When compared to other fabrication methods spray pyrolysis technique requires low temperatures, no vacuum, less power for the fabrication process and can be used for large-scale thin film deposition. (Eberspacher et al., 2001; Filipovic et al., 2013)

3.3.1 Synthesis of NiO Compact Thin Film

We have taken the cleaned and dried substrates, to begin with. We ultrasonicated the substrates in water for 3- 4 mins and cleaned them using a tissue. Substrates were then heated to 200℃ for 10 mins and allowed to cool down to room temperature. Once the samples were cooled down, they were used for further synthesis.

0.07M solution (~1.55 ml/ Substrate) of nickel acetate was prepared in Ethanol. The pH of the solution was adjusted to pH 4 by adding dil. HCL(2M) to the solution under constant stirring at nearly 2500 rpm on a hot plate. This was done at room temperature. Once solution pH was adjusted, it was allowed to stabilize on a hot plate at 60℃ (slowly increased from room temperature at 5℃/5 mins steps) for 2 hours under stirring at 2500 rpm speed. Airbrush was calibrated to a flow rate of 2ml / minutes at 2barr pressure using ethanol. A hot plate was taken, and a ceramic plate was placed on the hot plate to ensure uniform heat distribution. Cleaned substrates were placed on the ceramic plate and slowly the hot plate was heated to 290℃ (in 5℃/ min steps) (make sure that the substrate has 80ºC on the surface) and kept constant throughout the process. The solution was transferred to an airbrush and sprayed on the substrates from a constant distance of 15cm from the hot plate. The solution was sprayed for 10 secs and a delay of 1 min was given before the next spray. All solution was sprayed uniformly onto the substrates. The hot plate was turned off t the end and the substrates were allowed to cool down to 30℃ naturally before the substrates were taken from the hotplate. The ceramic plate along with the samples were then transferred to a hot air oven and kept at 80℃ for 1 hour and allowed to soft bake. The samples were taken out and allowed to come to room temperature. Samples were annealed again at 450℃ for 2 hours. The furnace temperature was increased from 30℃ to 450℃ at the rate of 4.3℃/ minute. The furnace was allowed to cool down to room temperature before samples were taken out of the furnace.

Figure 3.1

Synthesis of NiO Compact Thin films on Quartz Substrate

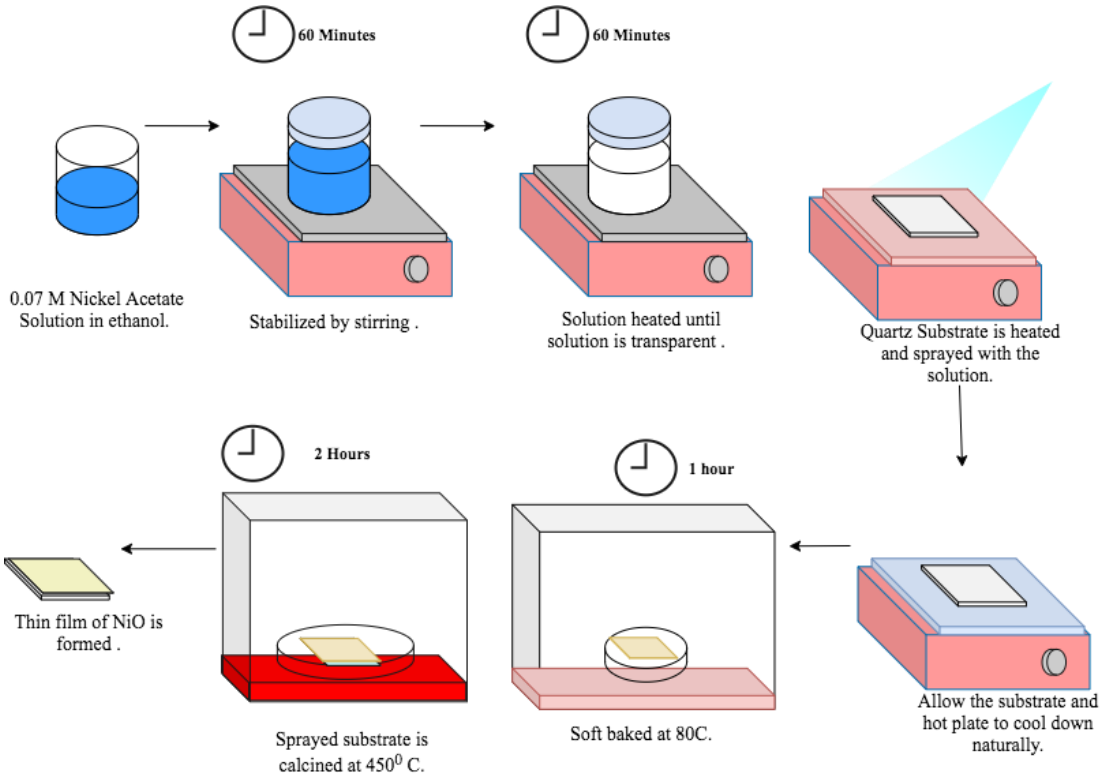

3.3.2 Synthesis of NiO Porous Thin Film

0.05M solution (~2.22 ml / Substrate) of Nickel Acetate was prepared in Ethanol. A procedure similar to the above synthesis steps is performed, the only changes are we use 0.05M solution and we spray in short pulses on the surface of the substrates. The solution was sprayed for 10-15 secs and a delay of 30-45 secs was given before the next spray. All solution was sprayed uniformly onto the substrates. The hot plate was turned off and the substrates were allowed to cool down to 30℃ naturally before the substrates were taken from the hotplate. The ceramic plate along with the samples were then transferred to a hot air oven and kept at 80℃ for 1 hour and allowed to soft bake, this step has helped in the formation of uniform thin films. The samples were taken out and allowed to come to room temperature. Samples were then transferred to a muffle furnace for annealing at 450℃ for 2 hours. The temperature of the furnace was increased from 30℃ to 450℃ in 2 hours.

Figure 3.2

Synthesis of NiO Porous Thin films on NiO Compact layer Quartz Substrate/ FTO Substrate.

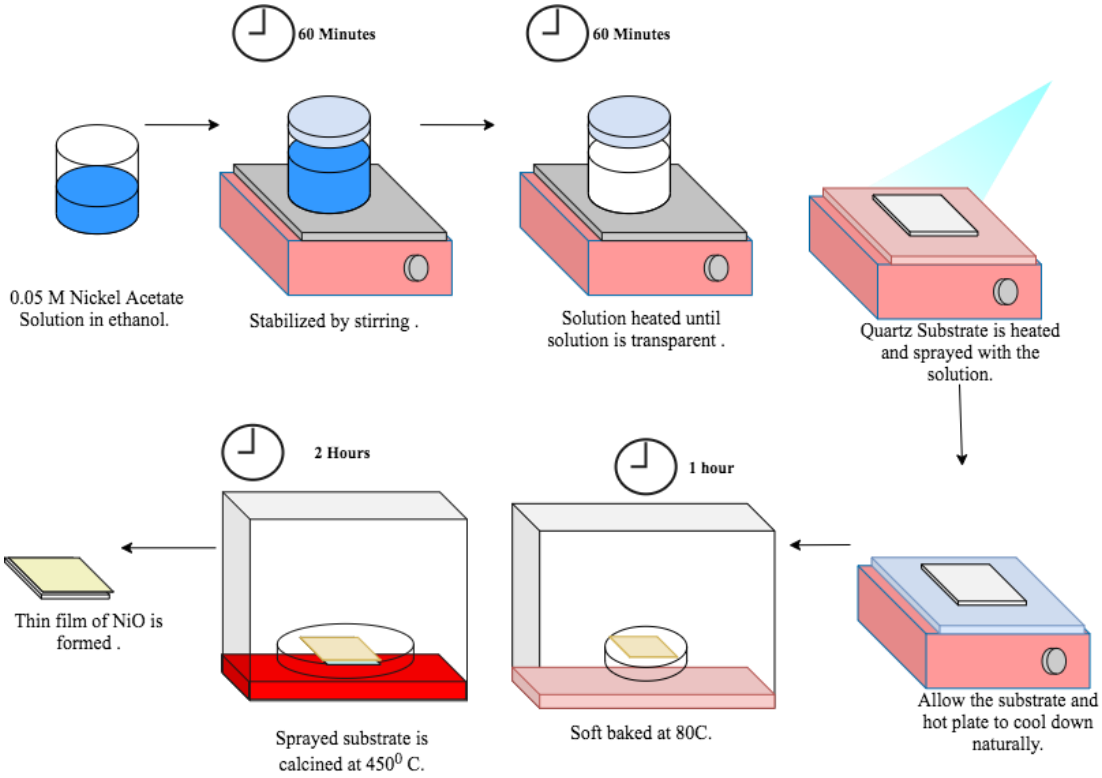

3.4 Synthesis of $NiTiO_3$ Thin Film on the NiO Thin Film

A modified spray pyrolysis coating technique (Phani & Santucci, 2001; Vijayalakshmi & Rajendran, 2012) was used to synthesize the $NiTiO_3$ thin film on the NiO thin film. This process has many advantages when compared to other techniques such as polymeric precursor (Lopes et al., 2009), co-precipitation (Gabal et al., 2013), and modified pechini method (Fan et al., 2012; Inceesungvorn et al., 2014; Lin et al., 2006a; Saito et al., 2020), stearic acid gel (Sadjadi et al., 2008), polymer pyrolysis(J. L. Wang et al., 2013). Advantages of using this technique are as follows: a) precise stoichiometric control, b) an increased rate of reaction, c) selective heating, d) environmentally friendly processing, e) greater reproducibility of the reactions, f) lower crystallization temperature, g) Low cost, h) scalable process, i) crack-free thin film j) semitransparent thin film. (Vijayalakshmi & Rajendran, 2012)

Experimental Procedure

0.01M nickel acetate and titanium isopropoxide (TTIP) (~ 4.27ml/ substrate) in ethanol were made. 0.06M (~ 4.27ml/ substrate) citric acid solution in ethanol was prepared

separately. Citric acid and TTIP solutions were added to a reaction flask and stirred vigorously. Slowly nickel acetate solution was added into the reaction flask and kept at constant stirring at 2500 rpm, 60℃ for 2 hours. The mixture was allowed to cool down to room temperature. Airbrush was calibrated to a flow rate of 4 ml/min at 2 bar pressure. A hot plate was taken, and a ceramic plate was placed on the hot plate to ensure uniform heat distribution. Cleaned substrates/ coated substrates were placed on the ceramic plate and slowly the hot plate was heated to 305℃ (in 5℃/ min steps) and kept constant throughout the process. The solution from the reaction flask was sprayed on all the substrates. The samples were allowed to cool down to normal temperature. Samples were allowed to soft bake at 80℃ for 1 hour in an air oven. Samples were then transferred to a muffle furnace for annealing at 600℃ of 4 hours. The temperature of the furnace was increased from 30℃ to 600℃ in 3 hours.

Figure 3.3

Synthesis of $NiTiO_3$ Thin Films. A Graphical Interpretation of Synthesis Process.

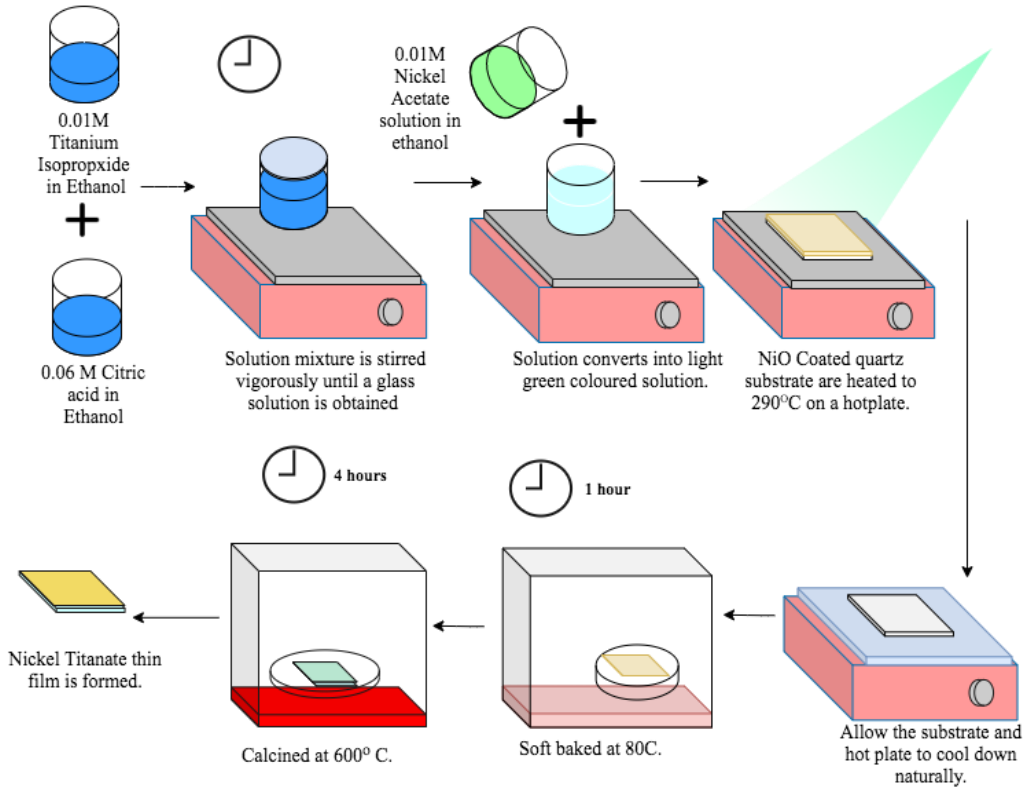

3.5 Characterization of the Thin Films

3.5.1 X-Ray Diffraction

X-ray powder diffraction (XRD) is an analytical technique mainly used for identifying phases of a material in the crystal and determining unit cell dimensions. We have collected the data by changing the angle of incidence of the X-rays. The diffraction patterns were compared to the data of the International Center of a Diffraction Database (ICDD) for getting to the conclusion of the lattice structure.

We have used XRD to determine the phase from the NiO, $NiTiO_3$ individual thin films, and Heterojunction. We have used the characterization facility at MTEC, (NSTDA, Thailand) for performing the XRD. The X-ray diffraction was performed on the Rigaku TTRAX III machine. We have used a Cu kα as a source for the X-rays ($\lambda = 1.5406$ Å). The sample was scanned from 20º to 70º of 2θ angles at a speed of 10º/minute. Data analysis was carried out using Powdll, Maud, and Qualx software, and XRD patterns were compared to the ICDD and Crystallography open database.

3.5.2 Scanning Electron Microscopy (SEM)

The surface morphology, grain size, average layer thickness was calculated from the cross-section of the heterojunction. The thickness of coatings helps us to realize the relationship between the photocatalytic degradation rate and the thickness of the photocatalytic coating. The sample was cleaned with DI water thoroughly and dried at 90℃ for 2 hours. The samples were sputtered with platinum, to make the surface more conductive, which results in higher clarity of the surface morphology. The gold coating makes it suitable for the analysis of the chemical composition using X-ray analysis. For the cross-section analysis, a sample was cut from one of the edges, and this sample was also sputtered with platinum. For the Scanning electron microscopy, Hitachi SU5000 FESEM was used. We have used the NCTC laboratory for performing FESEM. An accelerating voltage of 5 kV was used for imaging purposes. The magnification was varied from 5k to 100k for different images.

3.5.3 Energy-dispersive X-ray Spectroscopy (EDX)

EDX is an analytical technique used for characterizing and analyzing the elemental composition of individual thin films. In our study we have used this technique to study the elemental composition of the thin films, this helped us understand the thin film

composition. One of the most important aspects of this analysis would be the formation of the nickel titanate, as there is a possibility of the formation of nickel oxide and titanium oxide on the same thin film. Specific peaks at energies represent the presence of specific elements in the specific area of the nanostructure. A Horiba 70527 X-Ray Detector was used along with SU5000 FESEM. An accelerating voltage of 15kV was applied, with a magnification of 15000 X.

3.5.4 UV-Visible Spectroscopy

This is a simple spectroscopic technique that is used to determine the sample's optical properties. We have used absorption & transmittance spectroscopy to understand the optical bandgap of the material. This gave us an understanding of the optical bandgap of the material, thickness, uniformity of the thin film. The sample was exposed to well-calibrated light sources in the UV-Visible region of the electromagnetic spectrum. The changes in the light were observed to determine the material, quantity of material. Various materials absorb different parts of the visible spectrum. The spectrometer consists of a deuterium lamp that acts as a UV light source and a halogen lamp that acts as a visible light source. The absorption of the light by the sample is related to the bandgap of the material. We have examined the changes in the material, after being exposed to a wide range of humidity and photo exposure conditions. We have used the spectra suite software that comes bundled with USB4000 for analysis of the sample.

3.6 Stability Testing of the Heterojunction

The Heterojunction was tested for its stability in various light conditions for different intervals of time. We have exposed the heterojunction to different light sources namely UV light, Halogen light. Optical properties, electrical properties were studied using IV Characteristics (Current-Voltage), optical characteristics using UV-Visible spectroscopy.

3.6.1 Photostability Test

We have used a Philips (TUV 6W, G6 T5) tube light as a UV light source, Philips 50W halogen lamp as a visible light source, as different sources of light. The sample was placed at 10cm for UV-light and 15-20cm for halogen light. We placed the samples under the light for 24 hours (sampled every 6 hours) and samples were taken out and

characterized using UV-Visible spectroscopy, and an electrometer to study the change in optical and electrical characteristics of the heterojunction.

Figure 3.4

Photostability Test Setup.

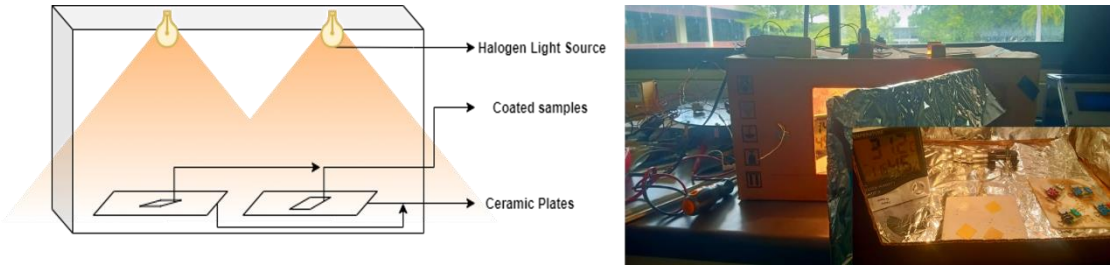

3.6.2 Stability against Humidity (R_H)

The heterojunction was tested against various humidity conditions by varying the relative humidity (60%, 80%). The heterojunction will be placed in a closed space and a smart humidifier kept inside, which creates and monitors the required humidity conditions. We then analyzed the changes in the electrical, optical of the heterojunction.

3.7 Characterization Techniques Set up and Procedures for Stability

3.7.1 UV -Visible Spectroscopy

We have used a USB 4000 module from Ocean Optics along with spectra suite software to perform the UV-Visible spectroscopy to find the changes in the optical response of the heterojunction samples after each test. The sample holder was cleaned thoroughly using dry tissue. The light source was turned on and the USB 4000 is connected to a system with spectra suite software installed. The standard procedure for obtaining the absorption spectrum was followed.

3.7.2 Electrical Current-Voltage (IV) Characteristics

We have determined the electrical characteristics of the heterojunction using an electrical setup, as shown in Figure 3.5. Voltage was varied using an electrometer (Keithley 617) from -2V to +4V with an increment of 0.05V at each step. The electrometer was also used to record the respective current value for the samples as we vary the voltage. A graph was plotted between the varying voltage and corresponding current values. Changes in the IV curve of the heterojunction gave us information

regarding the change in the electrical properties of the heterojunction. A computer was used to interface the electrometer.

Figure 3.5

A Mock Diagram of the Connections for the IV Curve Measurement of the Heterojunction Using Keithley -617 Electrometer.

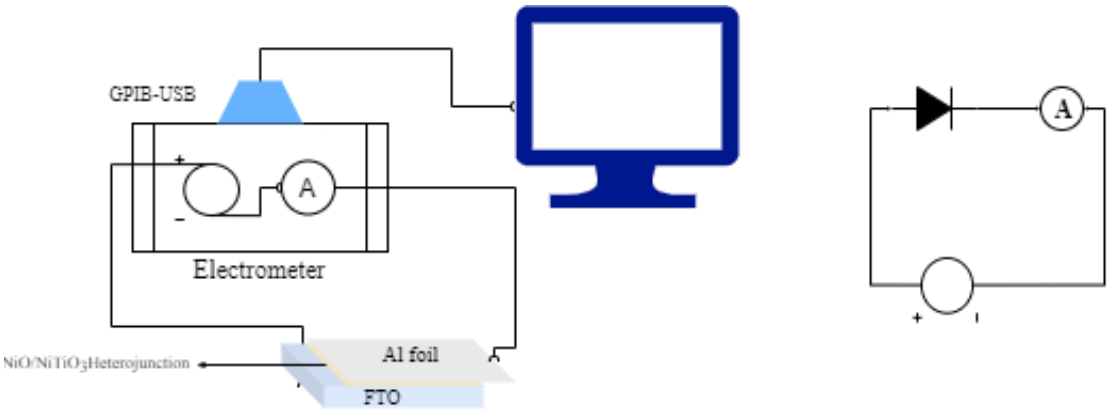

3.8 Photocatalyst Stability Analysis

3.8.1 Photostability

The IV curves of the heterojunctions were analyzed for the change in the electrical response. We found the difference by overlapping the IV curves on each other and tracking the difference in the IV curves. The heterojunction was called electrically stable in all the above conditions if there were no change (no significant change) in the electrical response of the heterojunction. We have analyzed the absorption spectrum for the changes in the optical properties. The heterojunction was called optically stable if there was no change in the optical response of the material. The heterojunction was called a photostable if there was no change in the electrical, optical properties of the heterojunction.

3.8.2 Stability Against Relative Humidity

We have analyzed the changes in the electrical and optical properties of the heterojunction similarly to the above-mentioned manner in the photostability section. But all the experimental procedures were followed in a closed environment, temperature and humidity were continuously monitored.

3.9 Photocatalytic Degradation Performance

For photocatalytic degradation performance testing, we have used various dyes Methylene Blue, Methyl Orange, Methyl Red (10mg/l) as samples of organic pollutants. We place our substrates in a beaker along with the model dye solution. Beakers were left in the complete dark for 90-120 minutes to complete dark reaction treatment. After 15 mins, a full-spectrum light source (halogen light source calibrated to give an intensity of 1000w/m^2, an equivalent to AM1.5 illumination of the sun) was turned on, which has provided a stable light illumination. The dye solution was collected at regular intervals of time (for every 15 mins) till 150 minutes of one full illumination. To eliminate the heating of the substrate we have used a water bath, placed between the light source and the samples. We have also used a convex lens to focus the beam of light straight onto the coating itself.

The absorbance of the collected liquid was recorded using a UV- Visible spectrophotometer. The decay of the model dye solution was be observed by determining the absorbance peaks for the solution by using the UV–vis spectrophotometer (at 470nm, 520nm, 661nm for Methyl Orange, Methyl Red, Methylene Blue respectively) using a glass cuvette. Peaks were observed between 400 and 700 nm, which are indications of the degradation of the model dye solution. From our understanding of Beer-Lambert Law, the concentration of dye solution is proportional to absorbance. Through this, we were able to calculate and quantify the photocatalytic degradation rate of the model dye solution. We have used the following equation for our calculations:

$$R = \frac{(C_i - C_f)}{C_i} \times 100\% \qquad (equation\ 3.1)$$

where, C_i is the initial concentration of the model dye in the solution and C_f is the concentration of model dye in the solution taken out at different times of the irradiation.

Figure 3.6

Photocatalytic Degradation Test Setup.

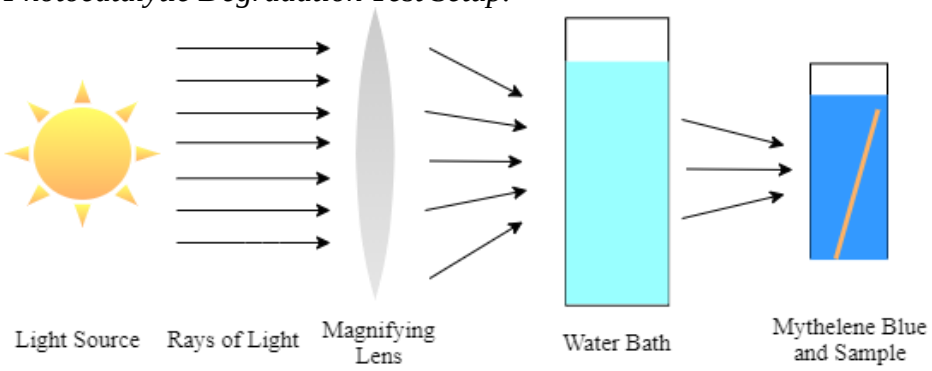

We quantified and compared the photocatalytic degradation efficiency over a fixed interval of time (150 minutes) using the percentage of the dye degraded. The three dye solutions would be compared in terms of the highest amount of dye degraded. We then estimated the degradation of each dye using two different light sources and 3 different dyes. We will be finding out the most effective photocatalyst from all the above-synthesized heterojunction and individual thin films. We have observed over the hypothesis of the study (i.e) how does heterojunction changes the photocatalytic degradation efficiency. We have also used the spectrometer to determine the photodegradation efficiency as a function of the absorbance of the dye in 470, 520, 660 nm for Methyl Orange, Methyl Red, and Methylene Blue, respectively. We also used this technique as a quantitative method to discuss and find the change in photocatalytic degradation of the dye.

CHAPTER 4
RESULTS AND DISCUSSION

4.1 Substrate Analysis

We have used silica fused quartz glass substrates as they have the most desirable optical and thermal characteristics which are the most desirable properties for the synthesis and development of the thin film Heterojunction photocatalysts. We have explored many options racing from uncoated ceramic tiles, porcelain, concrete, etc. We have found that the development of Photocatalytic heterojunction would be the easy and most economically viable method when we use silica fused quartz substrates, as we can use benchtop characterization techniques (UV-Visible spectroscopy) to study synthesized thin films. As our work mainly focuses on the optically active material thin films, silica fused quartz offers very high transparency in the visible region along with very high-temperature tolerance up to (1200^{o}C). We have performed some initial tests after receiving the samples. During our preliminary tests, the quartz substrate had no significant changes in the overall optical properties and did not have any damage visually, after treatment for 1 hour at 600ºC in a muffle furnace.

Figure 4.1

Transmittance Data for the Blank Substrate Before and After Annealing.

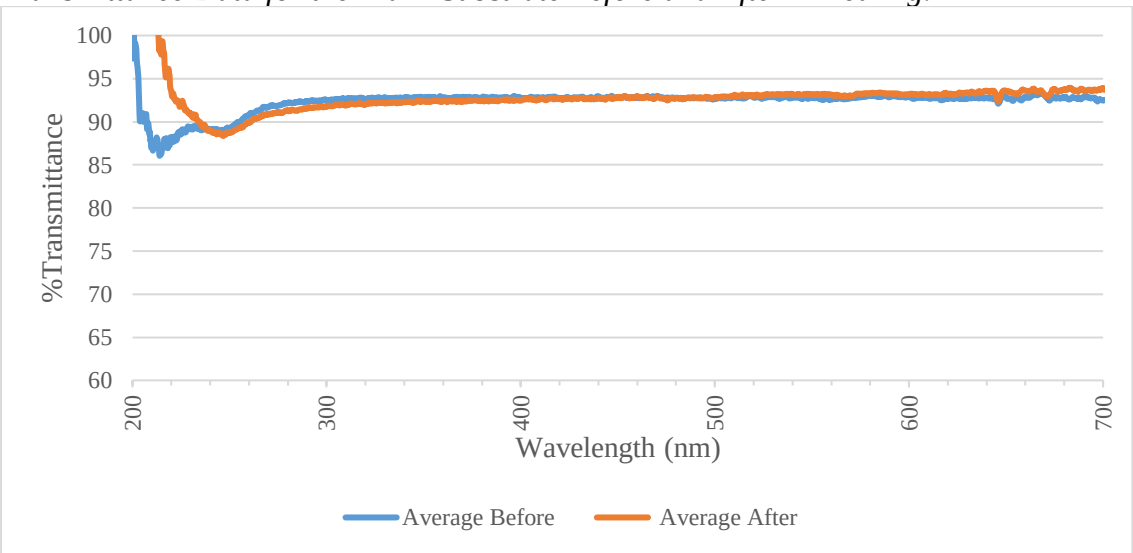

4.2 Nickel Oxide Thin-Film

A uniform thin film was deposited using the spray pyrolysis technique. We have coated the sample with a compact thin film followed by a porous, thin film. We have coated it with the compact thin film to prevent the heterojunction from shorting. A Porous layer was deposited using a higher flow rate and lower concentration. We have characterized the thin films using UV-Visible spectroscopy, X-ray Diffraction, and Scanning Electron microscopy techniques.

4.2.1 UV Visible Spectroscopy of NiO Thin Film

We have used deuterium and halogen lamps as sources of ultraviolet and visible light. Light Absorption was observed using a blank quartz substrate as a reference sample. NiO thin films had pale brown color in visual appearance after annealing in the muffle furnace. We have used UV-Visible spectroscopy to understand the material formed. A significant peak was observed at 320-325 nm, in all the samples, while the amplitude of the peak was varied in each sample. For each sample, readings were taken from 4 points and then averaged to get the final graph. The peak at 320 nm is reported in many works of literature, with this we have concluded that we could synthesize NiO thin films successfully(Mahmoud et al., 2011; Romero et al., 2010). The peak at 320 nm represents the bandgap of Nickel Oxide. We have previously observed the same peak consistently over the due course of repeated experimentation. The peak at 320-325 nm corresponds to the bandgap of 3.76 eV, which has been reported in many studies on NiO Thin films. During our study, we have found that substrate temperature and annealing temperature played a crucial role in the formation of highly crystalline thin films. Thin films synthesized at lower temperatures and higher pH were unstable and formed hydroxides.

Figure 4.2

(left) Blank Quartz Substrate ;(right) NiO Thin film

Figure 4.3

Absorption Spectra of NiO Thin Films

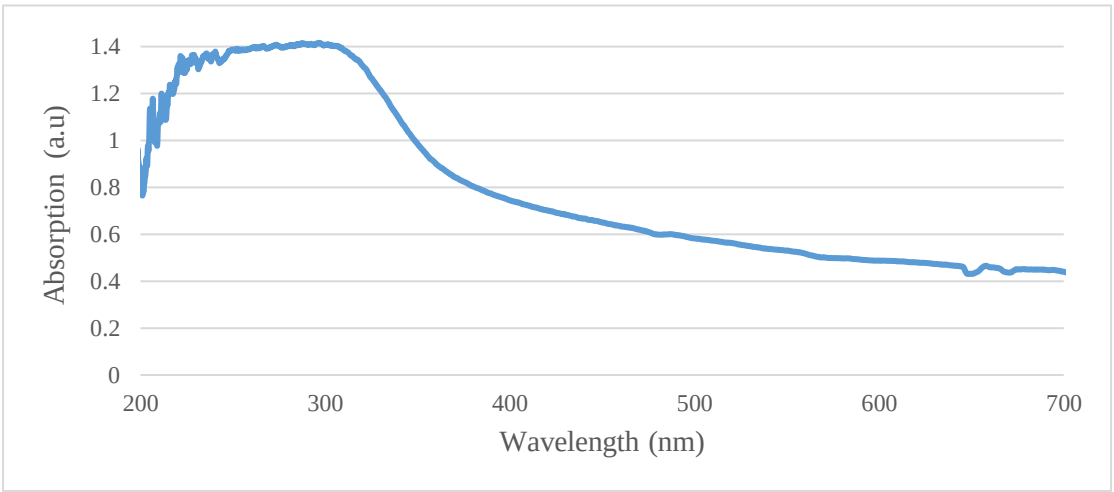

4.2.2 X-Ray Diffraction of NiO Thin Films

We have performed grazing incidence X-ray diffraction on NiO thin films with a Cu Kα X-ray as a source. We have observed the diffraction pattern from 20° to 70°, with a rate of 10° per minute. The data was converted into. XY file and we have done Rietveld refinement process by taking the observed data and compared to the ICDD database (ICDD-04-0835) and Crystallography Open Database (*Crystallography Open Database: Search Results*, n.d.; Thomassen, 2002)). There were high-intensity peaks observed at 37.2º, 43.2º,62º referring to (111), (200), and (220) planes, respectively. High peaks in the X-Ray Diffraction are due to the high crystallinity of the thin films. (Crystallography Open Database: Search Results .; Thomassen, 2002)

Figure 4.4

X-Ray Diffraction Data and Calculated Rietveld Fitted Curve.

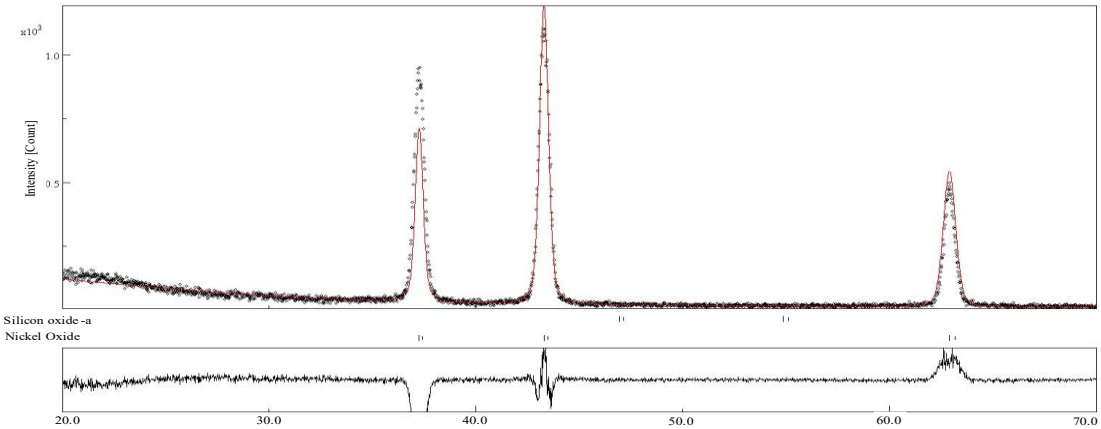

In the graph above (Figure 4.4) black dots represent the observed value from the experimentation. The red line is the fitted curve using Rietveld refinement by taking quartz and NiO X-ray diffraction patterns as a starting curve. After refinement, the calculated curve and the observed values have a very good curve fit. There is a shift in the peak positions, this is visible with two different lines, the longer line is the peak that is observed from the experimental value, while a shorter line represents the peak from the fitted curve.

4.2.3 Surface Morphology of NiO Thin Film

From the Scanning electron microscope, we have observed the uniformity in the surface and try to understand the surface morphology of the NiO thin films.

Figure 4.5

SEM Image of Top Surface Morphology of NiO Thin Film A) With Higher Magnification, B) & C) With Lower Magnifications.

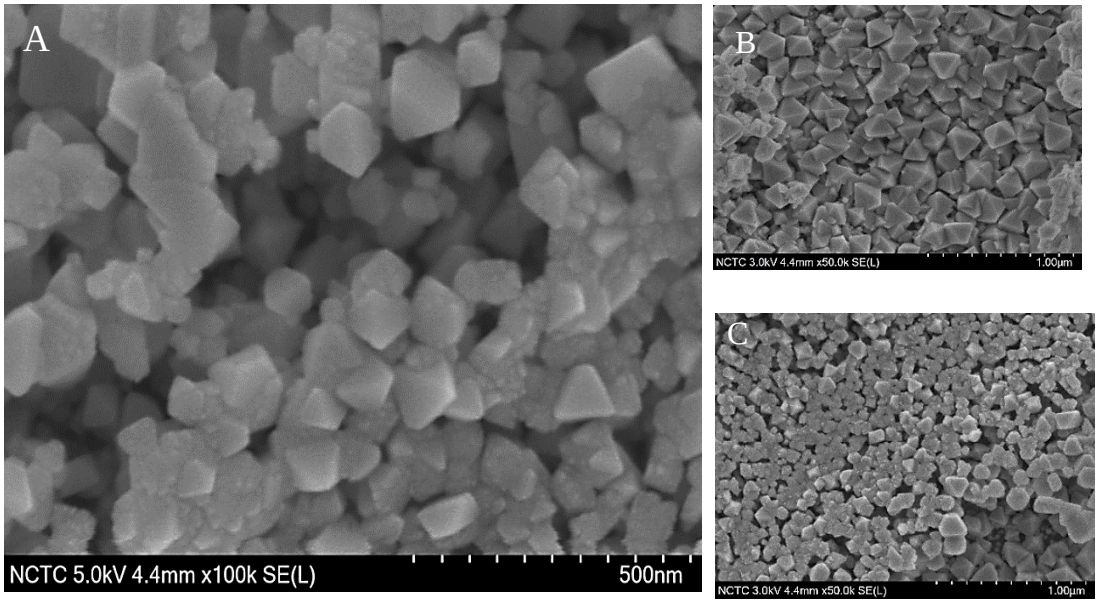

In the above figure, we can differentiate the crystals from the thin film surface. All the crystals have a very clear cubical structure. From the figure (B) and (C) we can observe that the film is not continuous rather the film is highly porous, with a decent distribution uniform sizes of the nanocrystals.

4.3 Nickel Titanate Thin Films

We have used the modified Pechini method for the synthesis of the $NiTiO_3$ thin films. We have not found any work, where this method was used to synthesize the thin films using this method. In all the other literature, this method was used to synthesize $NiTiO_3$ powders. In this work, we have tried to synthesize thin films by making a tweak in the synthesis method. We have used the same method for the preparation of the precursor solution. In powder synthesis, the precursor solution is slowly heated to evaporate the solvent and formation of the sticky gel, which is further calcined at a higher temperature, to obtain a ceramic powder with an extremely large grain size. We have used spray pyrolysis to coat the precursor solution onto a quartz substrate. We have noticed the formation of a sticky coating on the surface, similar to the traditional

modified pechini synthesis method. We have allowed the substrates to soft bake for 1 hour at 80C to remove the extra solvent from the substrate.

4.3.1 UV Visible Spectroscopy of $NiTiO_3$ Thin Film

$NiTiO_3$ thin films had bright yellow color in visual appearance after annealing in the muffle furnace. Peaks at 550nm and 770 nm-790 nm were observed in all the samples. These peaks are the representation of electronic transition between Ni to O transition and Ti to O transition. (Y. Qu et al., 2012) The flat peak at 310-320 nm represents the presence of the NiO phase from the Nickel Titanate thin film. (B. Yang et al., 2019) For each sample, readings were taken from 6 points and then averaged to get the final graph. From the calculation, we were able to obtain a bandgap of 2.18eV-2.2 eV, which is also found in many works of literature related to NiTiO3 synthesis. (Y. Qu et al., 2012; B. Yang et al., 2019)

Figure 4.6

Visual Appearance for Comparison, Blank Substrate (Left), NiO Thin Film (Middle), $NiTiO_3$ Thin film (Right).

Figure 4.7

UV Visible Absorption of Nickel Titanate Thin Film

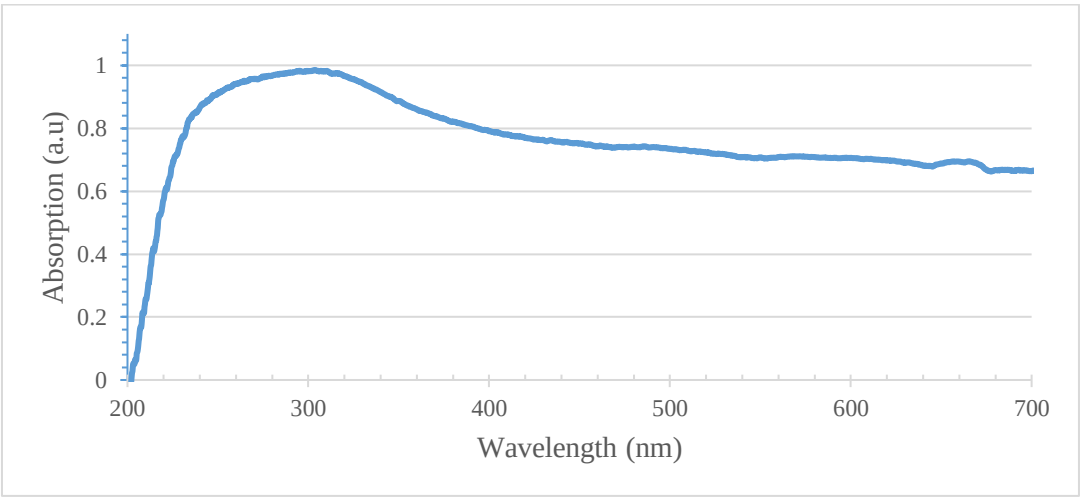

4.3.2 X-Ray Diffraction of $NiTiO_3$ Thin Films

From the figure 4.8 the black dots represent the observed values, while the red line represents the Rietveld fitted curve by taking the initial data from ICDD (ICDD file number – 04-006-6640, ICDD file number 03-065-118, ICDD file number 04-0835), and Crystallography Open Database. We observe clear peaks corresponding to the Rutile phase of TiO_2 (Rutile, and Anatase phase), NiO, and $NiTiO_3$. We have used the same device and all other parameters were kept constant as the measurement done for NiO thin films.

Figure 4.8

XRD of $NiTiO_3$ Thin Films.

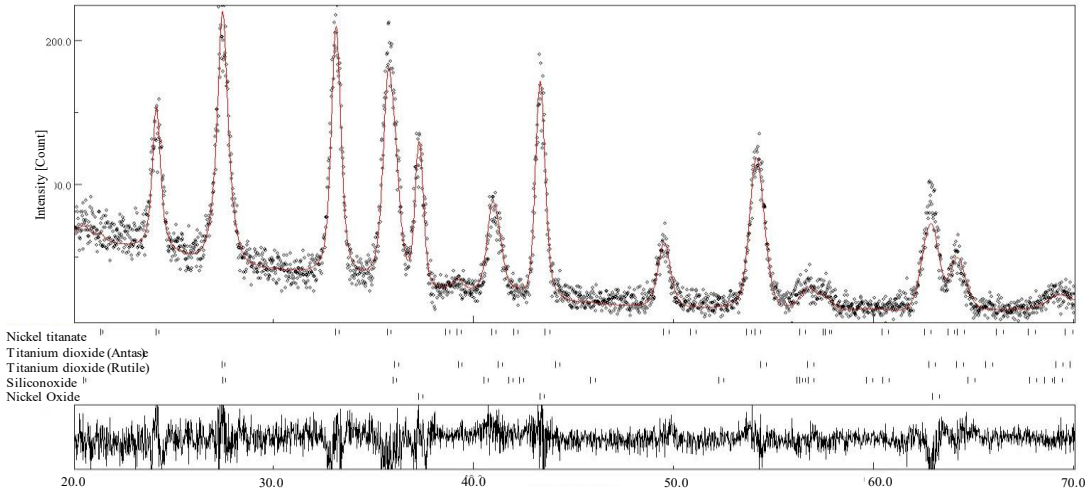

Table 4.1

Observed XRD Peak Angles and Calculated Angles from the Rietveld Refinement Method for the $NiTiO_3$ Thin Film.

No.	Angle observed	Angle Calculated	Material	Reference (ICDD)
1.	21.71	21.70	$NiTiO_3$	04-006-6640
2.	24.83	24.8	$NiTiO_3$	04-006-6640
3.	27.33	24.74	TiO2(R)	03-065- 118
4.	33.17	33.0	$NiTiO_3$	04-006-6640
5.	35.75	35.6	$NiTiO_3$	04-006-6640

No.	Angle observed	Angle Calculated	Material	Reference (ICDD)
6.	36.92	36.42	TiO_2(R)	03-065- 118
7.	37.07	37.2	NiO	04-0835
8.	39	40.9	$NiTiO_3$	04-006-6640
9.	41.17	41.5	TiO2(R)	03-065- 118
10.	40.9	41	$NiTiO_3$	04-006-6640
11.	43.31	43.2	NiO	04-0835
12.	44.32	44.40	TiO_2(R)	03-065- 118
13.	49.58	49.4	$NiTiO_3$	04-006-6640
14.	54.24	54.65	TiO_2(R)	03-065- 118
15.	56.82	56.56	TiO_2(R)	03-065- 118
16.	57.61	57.4	$NiTiO_3$	04-006-6640
17.	62.79	62.5	$NiTiO_3$	04-006-6640
18.	62.97	62.8	NiO	04-0835
19.	64.12	64.19	TiO_2	03-065- 118
20.	64.23	64.20	$NiTiO_3$	04-006-6640
21.	69.12	69.26	TiO_2(R)	03-065- 118
22.	69.70	69.83	TiO_2(R)	03-065- 118

From the XRD data, we can clearly say that the film had mixed phases of Titanium dioxide (rutile), Nickel Oxide, Nickel Titanate. Our results are comparable to the results reported by other researchers working on NiO/TiO_2 Heterojunctions, and synthesis of $NiTiO_3$ thin films. (Lin et al., 2006b; Rawool et al., 2018)

4.3.3 Surface Morphology of $NiTiO_3$ Thin Film

Figure 4.9

Surface Morphology of Nickel Titanate Thin Films a) Higher magnification, B) Lower Magnification.

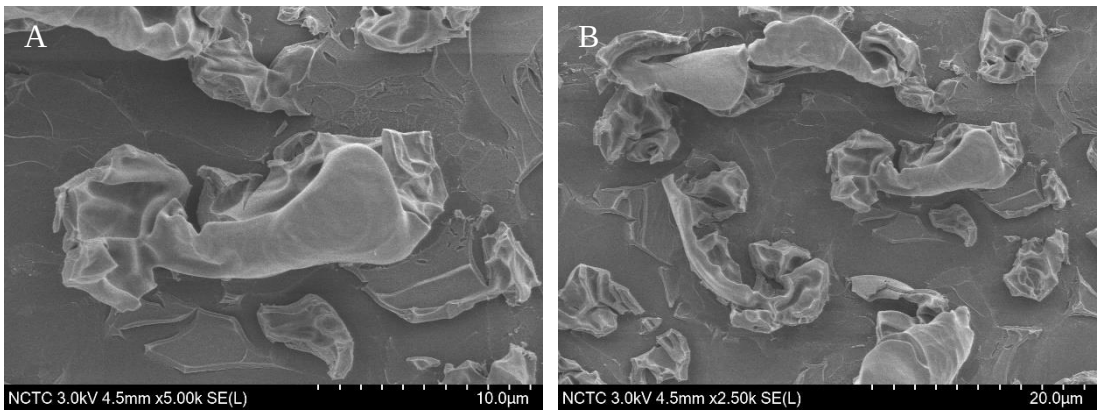

From the SEM images, we can see that microstructures with an average size were formed along with the thin film. From the image, it is clear the particles are not in a perfect shape rather they have random shapes and like the chipped-off thin film with cracks. Upon further observation, they were spherical-shaped particles that was that made up the bigger agglomerated particle. Some of the key factors responsible for the random shape and the cracked film are higher temperatures of synthesis, incomplete evaporation of the solvent. Agglomeration would be because of the higher annealing temperature around 600º C, and strain caused by the cracks of the film. We can further optimize the synthesis parameters such as substrate temperature, reduced flow rate, increased pressure, and longer soft baking period to ensure that we get a uniform thin film. We have also observed that Nickel titanate has very little adhesion to the substrate resulting in a coating like the thin coating of dust on the glass surface. A gentle wipe was enough to remove the Nickel titanate thin film.

4.4 NiO / $NiTiO_3$ Heterojunction

We have synthesized a heterojunction by performing 2 step spray pyrolysis and annealing steps. We have successfully synthesized a heterojunction with NiO and $NiTiO_3$. We confirm the formation of the heterojunction from the I-V curve obtained with the help of an electrometer.

4.4.1 Electrical Characterization

I-V Curve obtained resembles a diode characteristic. From the I-V curve, the reverse breakdown voltage was measured at -1.9V and the heterojunction shows an ohmic character from 1.85 V- 2.0 V.

Figure 4.10

I-V Curve of $NiO/NiTiO_3$ Heterojunction.

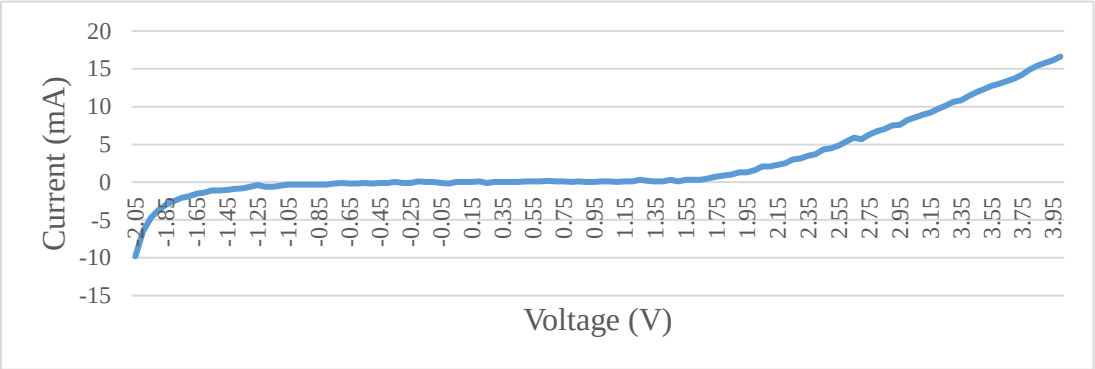

The IV curve shows very small currents followed by a linear region. After a voltage of 1.8V, the voltage increases linearly. The sample was behaving like a PN diode, Where NiO was acting like a p-type material and $NiTiO_3$ acts as an n-type material. FTO glass acts as one of the electrodes and aluminum acts as another electrode. The samples were tested multiple times but there was no change in the response of the sample. We have tested multiple samples, almost every sample gave a similar I-V curve.

Figure 4.11

Band Bending Diagram and Formation of Heterojunction.

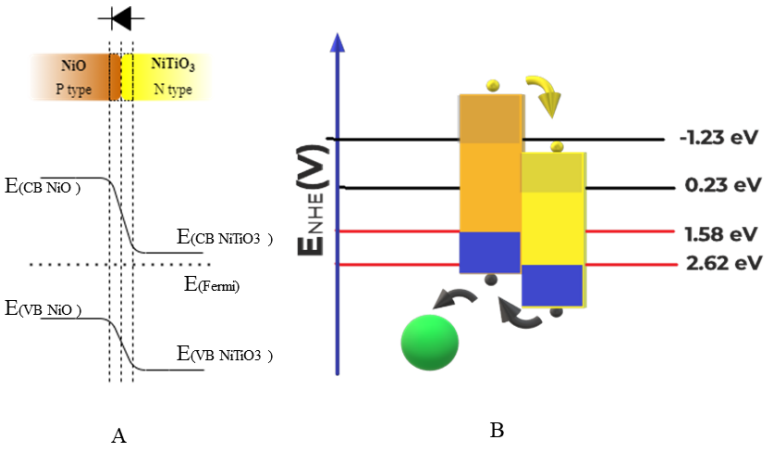

From figure 4.11 figure a represents the formation of the P-N junction and adjustment of the energy band of material. Nickel Oxide has its conduction band edge at -1.23eV and Nickel Titanate has its conduction band edge at 0.23eV. Similarly, Nickel Oxide has its valence band edge at 1.58eV and Nickel titanate has its valence band edge at 2.62eV. Generally, the fermi level energy of P-type material (in our case Nickel Oxide) has its fermi level closer to its valence band, due to its intrinsic bandgap formed because of the overlapping of the molecular orbitals. While the Fermi level in an N-Type material (in our case Nickel Titanate) is closer to the conduction band. When two materials are brought closer, they result in the drifting of charge carriers to the heterojunction forming a potential gradient across the cross-section of the material. Due to the accumulation of these charges, there is a barrier potential that is formed. When an external potential is applied there will be a shift in the energy bands of the system. When a positive voltage is connected across the junction, there is a minimum flow of electricity until a particular positive voltage and then when voltage is increased further the current increases exponentially. After this point, the device behaves like an ohmic device (resistor). The main reason for exhibiting such behavior is the reduction of the depletion region across both sides of the semiconductor. After the knee voltage, the depletion region is completely gone, thus resulting in the free flow of charge carriers. In the above-mentioned graph (figure 4.10) the knee voltage is observed at 1.85-1.9 V and After 2.25V the heterojunction started behaving as an ohmic junction. When a negative potential is applied the opposite phenomenon happens the width of the

depletion increases rapidly until the device reaches a very high electric field, such that the device breaks down and starts to behave like a conductor. This voltage at which the device breaks down is called a reverse break down voltage. From figure 4.10 the reverse breakdown voltage is observed at -1.9V. From the above observations, we can conclude that we have successfully synthesized the heterojunction.

Figure 4.11 (B) gives us a mechanism of photocatalytic activity, because of the formation of the heterojunction.

4.4.2 UV Visible Spectroscopy of $NiTiO_3$ Thin Film

Visually the samples have a deeper yellow along with a pale brown tinge.

Figure 4.12

Photograph of All the Samples Side by Side. Blank Substrate, NiO Thin Film, $NiTiO_3$ Thin Film, NiO/$NiTiO_3$ Heterojunction. (Left to Right)

Figure 4.13

Absorption of NiO/$NiTiO_3$ Heterojunction

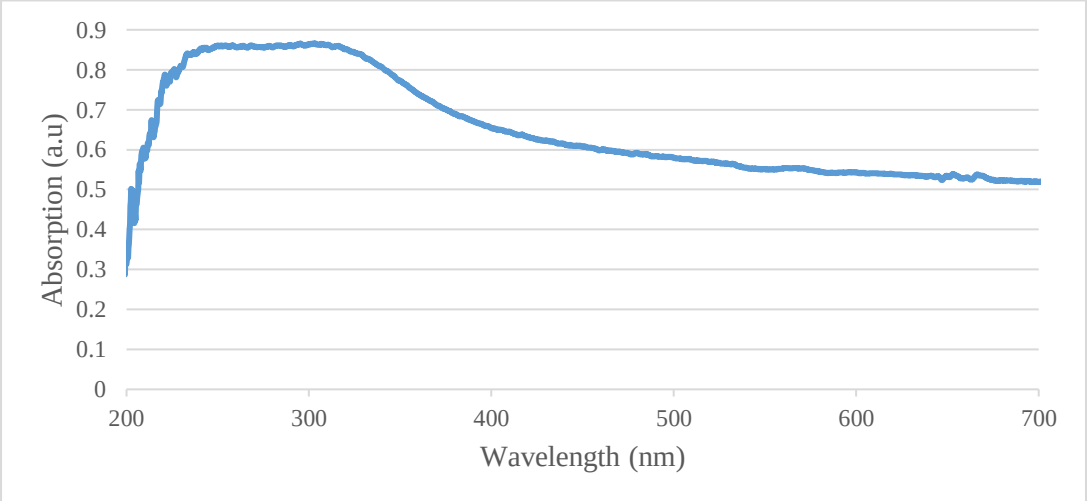

The flat edge at 320nm represents the presence of Nickel Oxide. While there were very less variations elsewhere in the graph. We could not find the corresponding transitions of Nickel Titanate in the UV Visible graph. We have performed XRD to understand the composition of the thin film.

4.4.3 X-Ray Diffraction of NiO/ $NiTiO_3$ Heterojunction

We have performed X-ray diffraction for the heterojunction sample. we have used the same conditions and same instrument without any changes in the device's configuration.

Figure 4.14

X-Ray Diffraction Pattern Along With Rietveld Refined Curve of Heterojunction.

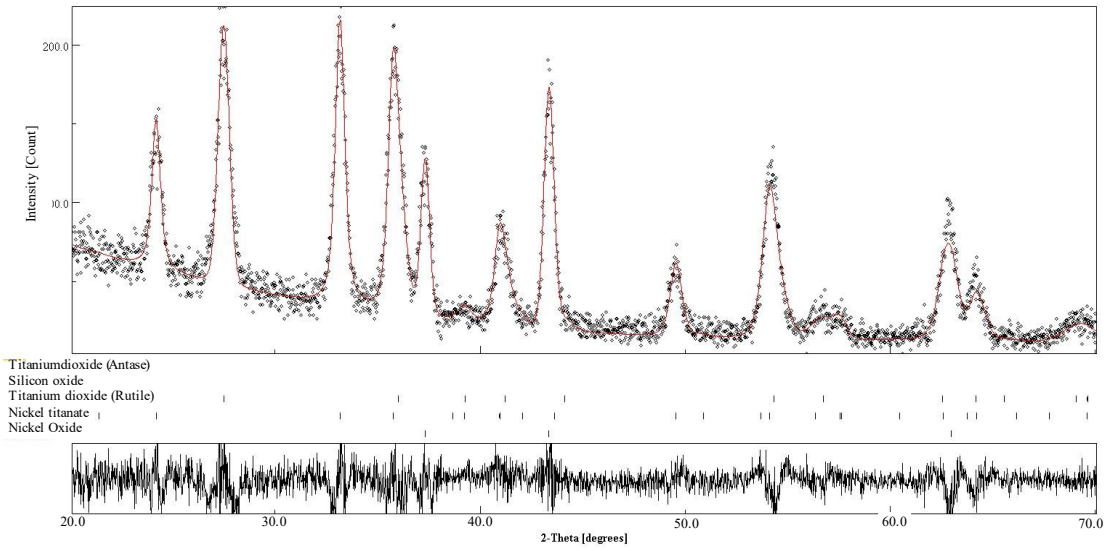

From the above graph, we can identify the peaks for TiO_2 (Rutile), NiO, and $NiTiO_3$, like the XRD pattern, which was observed with $NiTiO_3$. All the peaks were the same, except the phases of NiO are having a greater peak. This is due to the higher presence of the crystalline NiO Thin Films. The results of X-ray diffraction are following our data that has been observed using UV-Visible data.

4.4.4 Surface Morphology and Cross-Sectional SEM

We have performed Scanning electron microscopy to understand the surface morphology and Cross-sectional SEM to understand the film thickness and heterojunction formed. We have found that there are no uniform thin films formed at

the heterojunction while Heterostructures were observed on a layer of NiO crystals. These heterostructures had different phases of titanium dioxide and nickel oxide instead of pure nickel titanate. Samples were also analyzed using EDS to ensure that there were no impurities present and understand the composition of the complex heterostructure formed.

Figure 4.15

Scanning Electron Microscopy Images (A) Higher Magnification, (B), (C) Lower Magnifications.

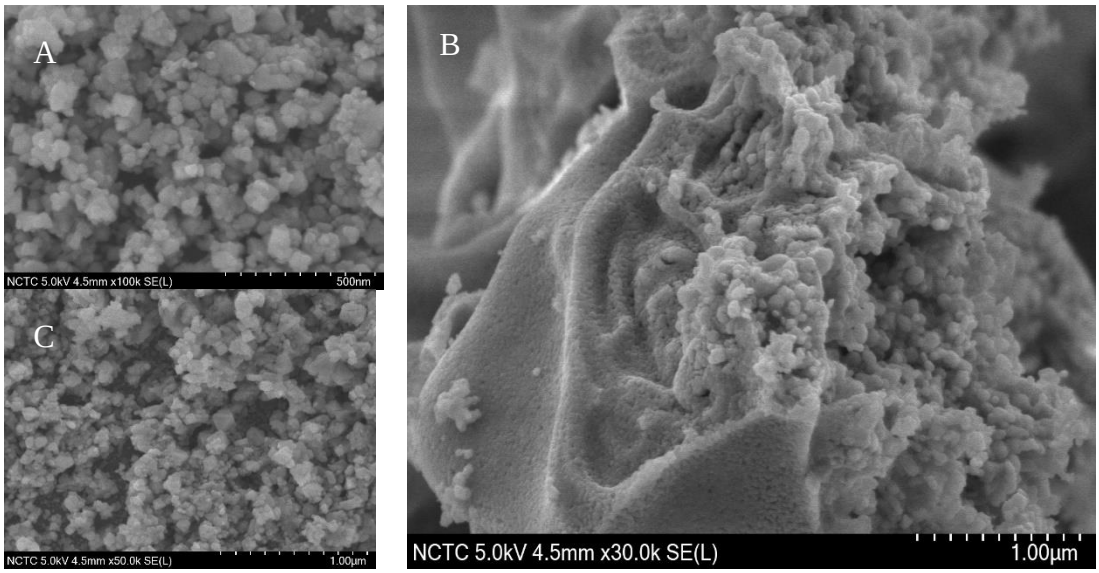

From the above image (Figure 4.15), B is the higher resolution image of the complex heterostructure. In the image on the left side, there is a structure like the structures observed in the SEM images of the $NiTiO_3$ thin films. While the structures in the right are like the nanostructures observed in the NiO thin film SEM images. From figure 4.15 A and C we have found that the nanostructures have similar morphology that we have observed in the NiO thin films (cubic shaped crystals). The microstructures on the solid structure are appearing to be porous. In figure (A) we can observe small nanostructures around 45nm (spherical) consisting of complex structures. We think the bigger particles are a result of the agglomeration of the small nanostructures.

Figure 4.16

Scanning Electron Microscopy of Cross-section of Heterojunction. A) 5k Magnification Along With Marked NiO Layer. B) 7k Magnification Along With Marked NiO layer.

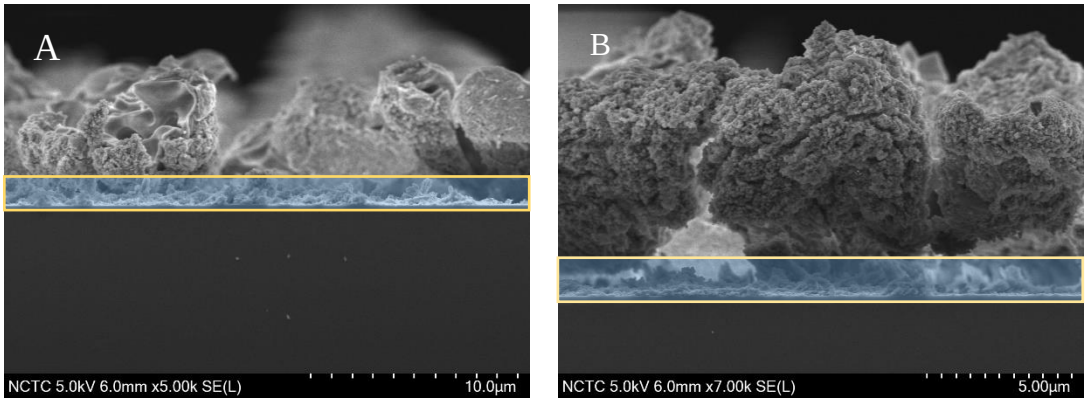

From the above Figure 4.16, we can observe heterostructure, the lower sides of the microstructure were completely covered smaller nanostructures. The Nickel titanate structure is encapsulated with smaller NiO nanoparticles. The structures resembled coral reefs that grow on the stone, where the corals are the NiO nanostructures and $NiTiO_3$ structure being the rock. We have confirmed this from different parts of the heterojunction sample. We have taken images from two different points of the sample under SEM (from the above image A & B). The rectangular box is the NiO layer in both images.

Figure 4.17

EDS Spectrum of Different Parts of the Nanostructure. A) SEM Image with 3 Areas Marked; B) EDS Spectrum of Area 1; C) EDS Spectrum of Area 3; D) EDS Spectrum of Area 2.

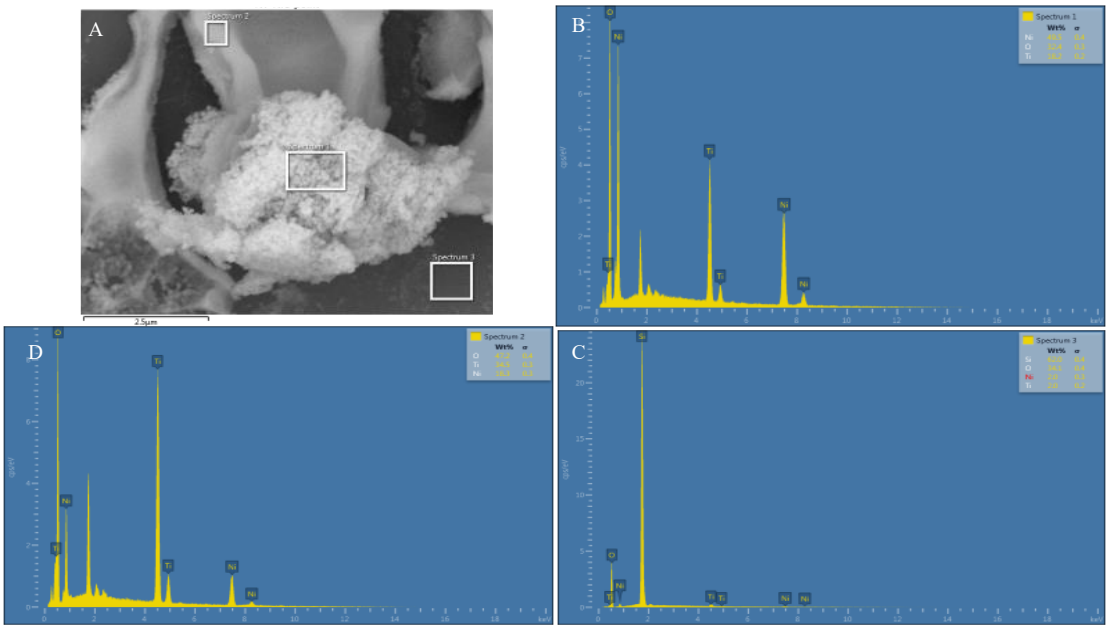

Figure 4.17 (A) is the SEM image, and three boxes represent 3 regions of the sample. The box in the middle of the image represents spectrum 1, the box on the left top represents spectrum 2, box on the right represents spectrum 3. We have used EDS to find the composition of the nanostructure. All the compositions are expressed as the percentage of weights of each element. In region one we have observed is 49.5% of Ni, 32.4% of O, 18.2% of Ti. From the image in region one, there is a maximum percentage of NiO phase. In region 2 we have observed 47.2% oxygen and 34.5 % of Ti and 18.3 % of Nickel. There is a higher probability of $NiTiO_3$ in this region. From the image, the nanostructure is also like the structures observed in that $NiTiO_3$ thin films. In region 3 we have observed 62% of Si, 34.1% of Oxygen, and small amounts of Nickel. From the image, we can conclude that the weight percentages, can be the composition of the quartz substrate along with NiO on it.

Figure 4.18

Elemental Map of the composition of the nanostructure.

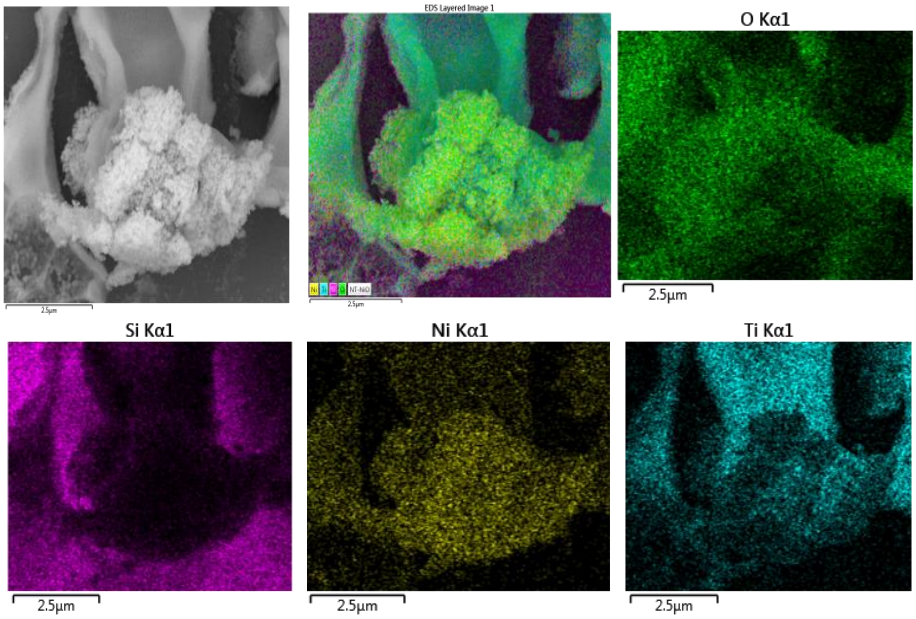

From Figure 4.18, we correlate and understand the distribution of the elements across the sample. These images along with SEM and XRD data give us a very good idea about the composition and distribution of the thin film heterojunction.

From all the above thin film characterization results we hereby conclude that we have been successfully synthesized high-quality NiO thin films using spray pyrolysis in all ambient conditions. While we have also successfully synthesized the $NiTiO_3$ thin films, but we have mixed phases of NiO and TiO_2. The molar ratio of the precursors for the synthesis of Nickel Titanate thin films has a significant effect on the formation of the Titanate phase. Annealing temperature, molar ratio, and citrate concentration have a significant effect. Morphology of titanate is highly dependent on the spray rate, flow rate, substrate temperature, soft baking time, annealing temperature, cooling rate after spraying of the precursor, rate of the increase in temperature for annealing, Annealing time. Our results are very comparable to the results reported by other researchers in this field. Even today synthesis of pure titanate is challenging.

4.5 Photostability

We have checked for the stability of the Heterojunction underexposure of Visible light and UV for 24 hours, sampled every 6 hours. We have observed changes in the electrical properties and optical properties. An average of 250w/m^2 was irradiated using a halogen lamp. The temperature was not controlled, and the maximum temperature went up to 45ºC, humidity was not controlled. A stability test was performed in all ambient conditions.

4.5.1 Photostability under Visible Light

Samples were kept 15 cm away from the light source. Samples were kept on a ceramic plate (acts as a heating sink) and prevent samples from overheating. Every 6 hours that samples were taken out and UV -Visible absorption spectra were obtained. From the Absorption spectra, there was no change in the visible region and UV region. While the abnormalities in the observed spectra are due to the nonuniform coating and errors from the UV-Visible Spectrometer's optical fiber. The heterojunction was found to be optically stable under constant exposure of the sample to the light for 24 hours.

Visually there was no change observed in the color or texture of the film with the naked eye.

Figure 4.19

Absorption Spectrum of $NiO/NiTiO_3$ Photostability Visible light.

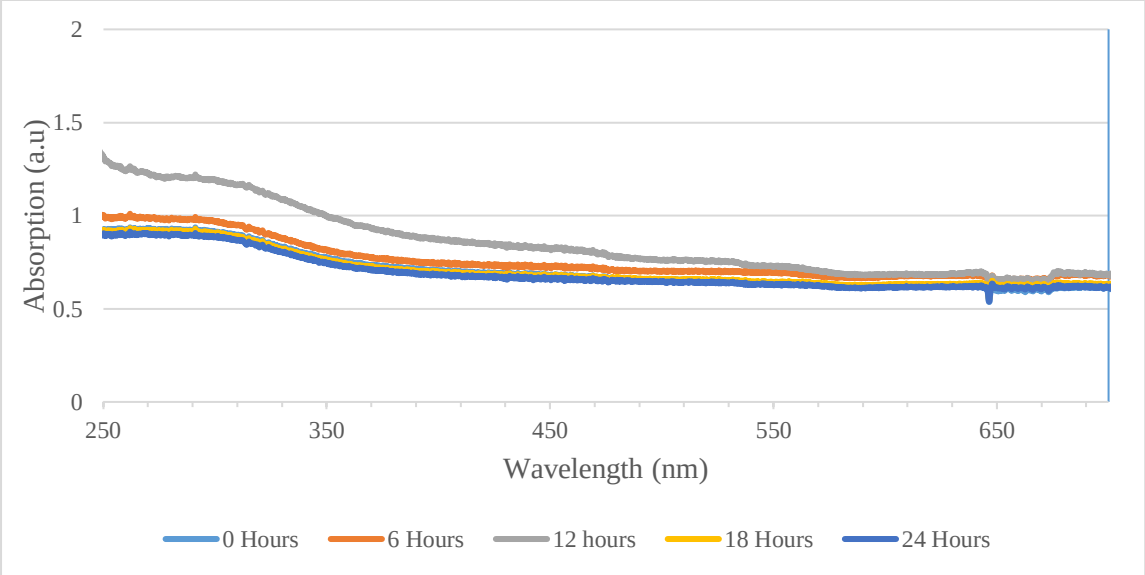

Figure 4.20

I-V Curve of Heterojunction Photostability Visible light.

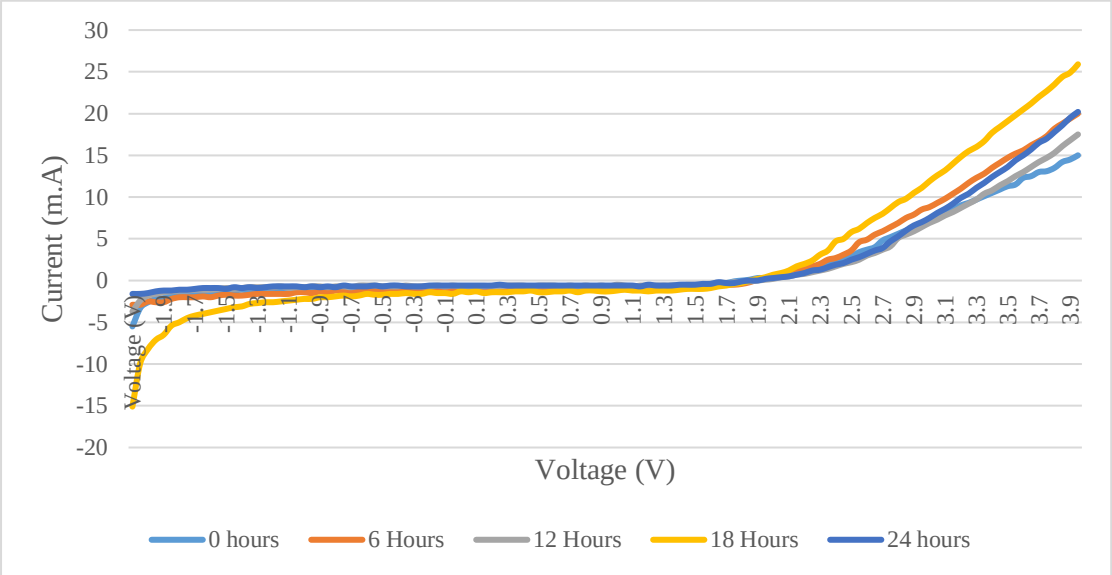

We have used a Keithley 610 Electrometer to measure the I-V curve. The voltage varied in steps of 0.05V and corresponding current values were recorded. We have used crocodile clips to connect the samples to the electrometer. The contact between crocodile clips and samples resulted in slight variations in the recorded data. While the knee voltage and reverse breakdown voltage remained constant. This helps us to conclude that the heterojunction was stable under constant illumination of visible light.

With the above results, we can conclude that the heterojunctions were stable in terms of optical properties and electrical properties when heterojunction is exposed to the lighting condition. We can further extend the study of photostability over a period and with varying light intensities. Due to the limited time, we have performed initial stability tests to understand the photostability of the coatings.

4.5.2 Photostability under Ultraviolet Light

We have used a UV-C lamp as a source of light. We have used a UV curing chamber for this purpose. Samples were kept at nearly 10 cms from the source of the light. A similar procedure to the visible light stability test was followed.

Figure 4.21

Absorption of $NiO/NiTiO_3$ Photostability under UV-C.

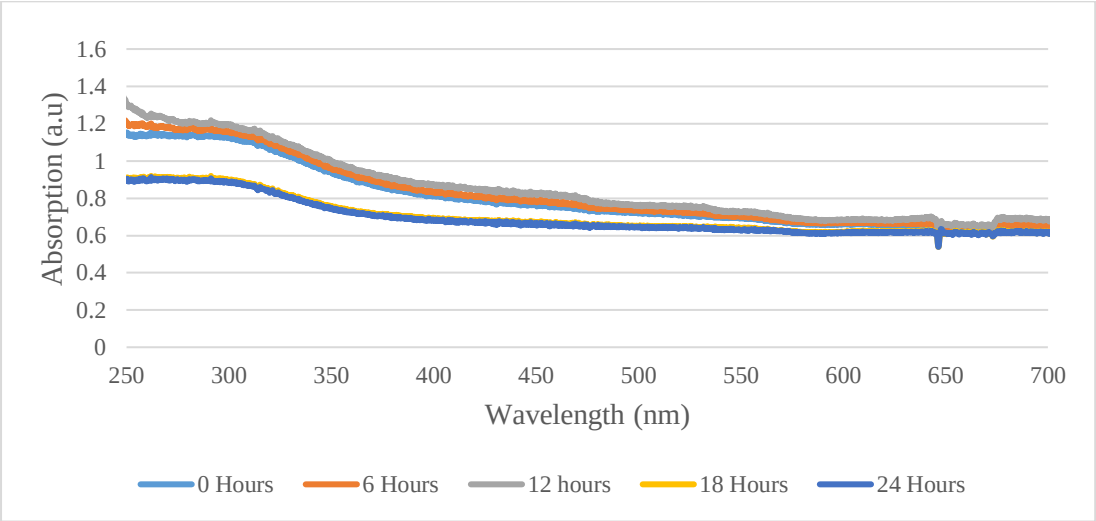

From the above graph from figure 4.21, the sample is stable as there is no change in the absorption peaks that were observed after the exposure of the samples to UV Light. The change in the absorption values is due to the non-uniform coating. There were no changes in the absorption peaks that were observed.

Figure 4.22

IV- Curve of Heterojunction Photostability Under UV-C

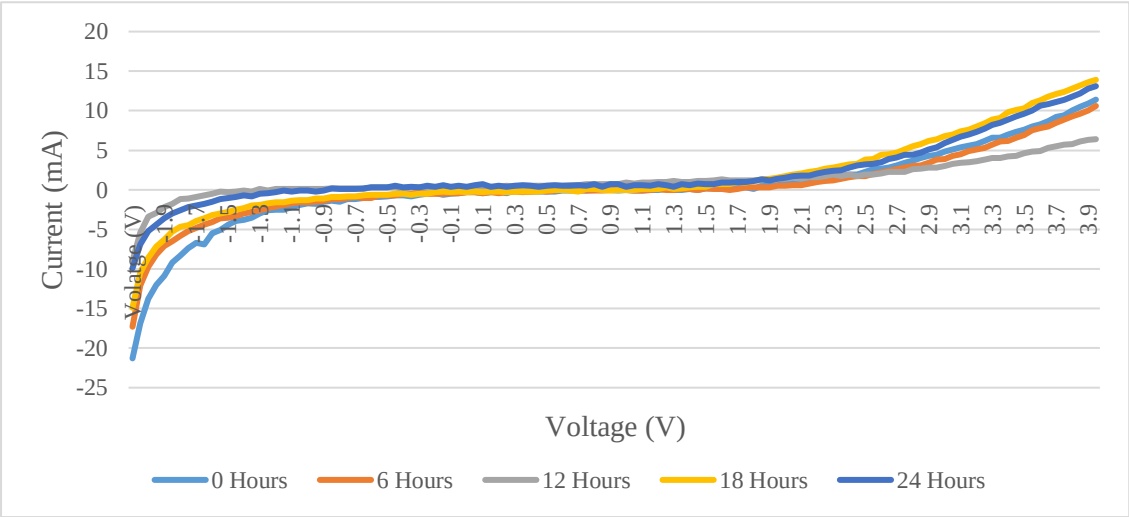

From the above graph, the breakdown voltage and knee voltage are remaining constant while resistance in the ohmic region increases.

With the above results, we can conclude that the heterojunctions were stable in terms of optical properties and electrical properties when heterojunction is exposed to UV

light. From the above tests, we have concluded that the heterojunction is stable under visible light and UV light. The heterojunction formed is photostable.

4.6 Stability Under Different Humidity Conditions

We have performed the stability tests for the samples for 2 different humidity conditions (i.e) (60% RH, and 80% RH). The samples were found to be stable after days of synthesis when stored at normal room temperature and stored in the open air. We have used a digital ultrasound humidifier with an automatic humidity controller to maintain constant humidity conditions. The samples were kept on and ceramic plate and kept in an enclosure made of acrylic. Samples were taken out of the chamber after every 6 hours and sampled for the changes in the optical properties and electrical properties. A similar method followed for the photostability was used for testing the samples for stability for humidity conditions.

Figure 4.23

IV Curve of Heterojunction After Exposure to Humidity of 80%RH.

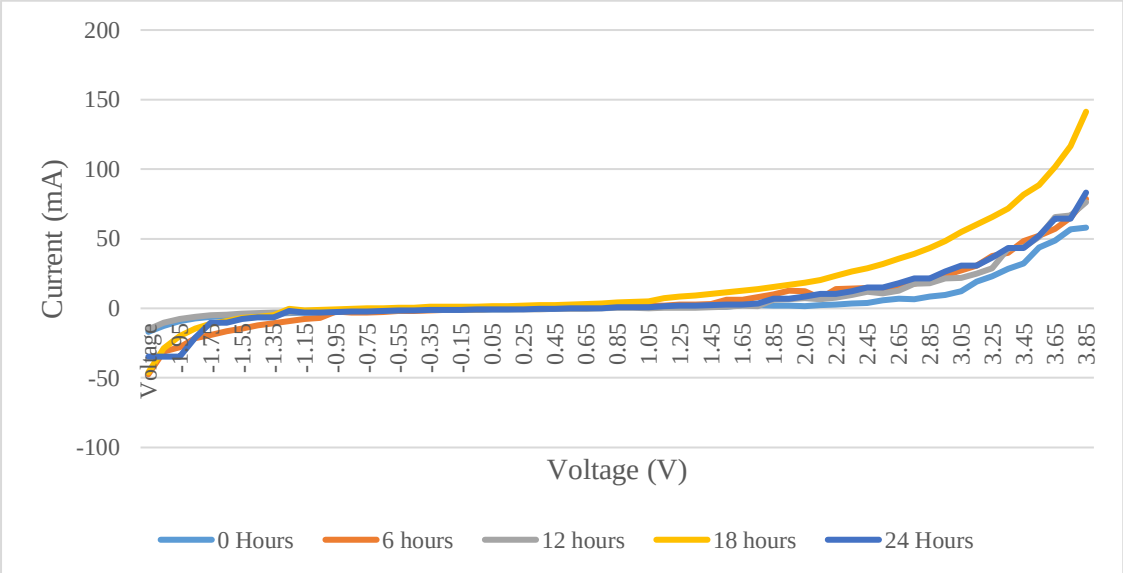

Figure 4.24

Threshold Voltage vs Exposure Time (80% RH)

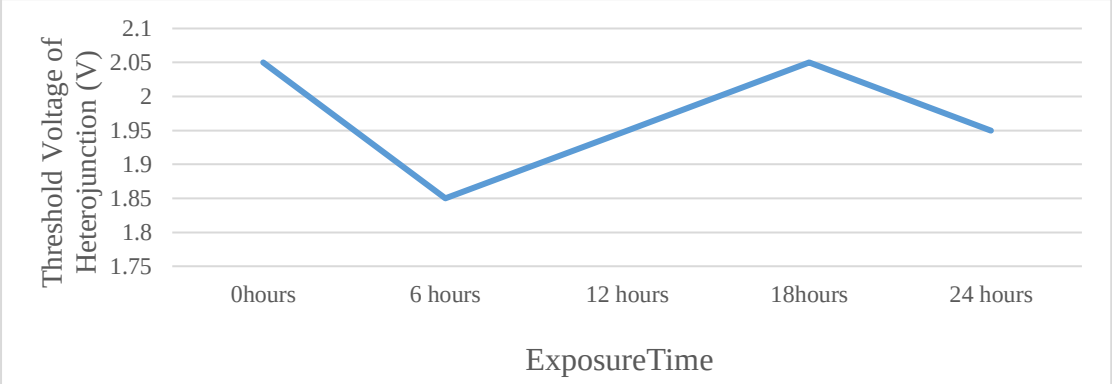

From figure 4.23 and figure 4.24, we were able to observe that the I-V curve (Threshold voltage and break down voltage) were almost the same. There was no significant change in these values. So, from the above, we can say that heterojunction was stable under constant exposure to very high humidity conditions.

Figure 4.25

UV Visible Absorption After Different Time Intervals of Exposure to 80% RH.

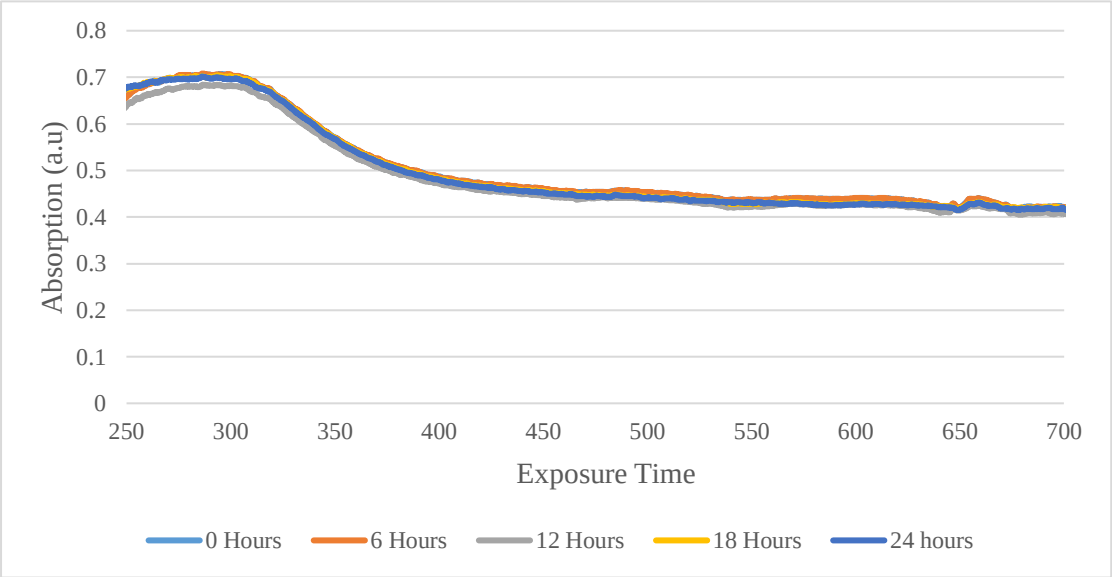

From figure 4.25, we observe that there is no significant difference in the peaks. And there is no change in the sample visually in terms of texture and color. Hence, we can say that the heterojunction is having great stability (optically and electrically) when

exposed to higher humidity conditions. The response in the visible region is constant trough out.

As the sample was stable, we have used the same sample for testing the stability at 60% RH as well. (Only quartz sample was reused).

Figure 4.26

I-V Curve of Heterojunction After Exposure to 60 % RH.

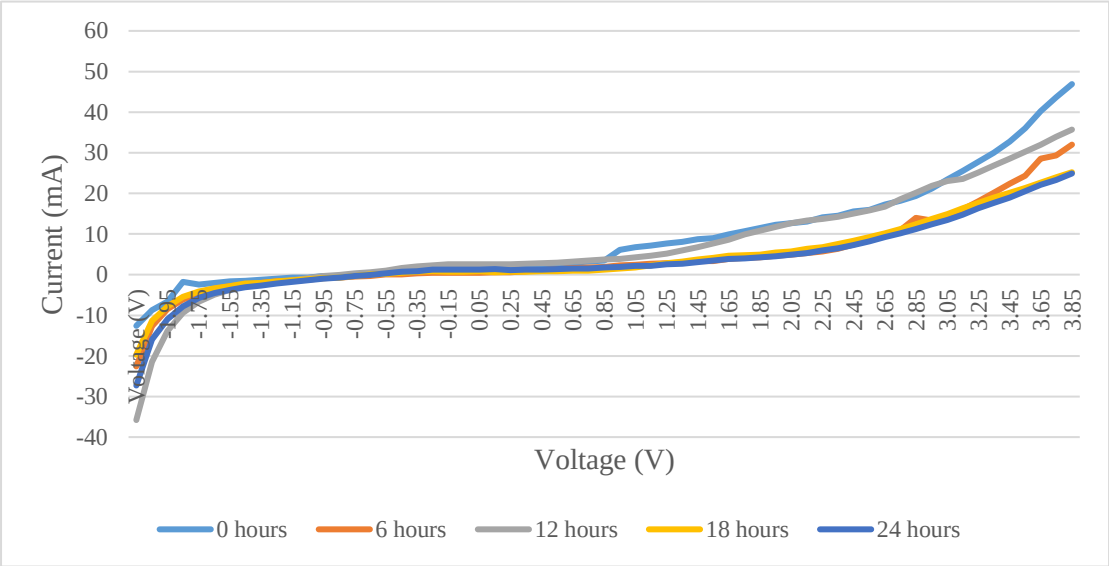

From the above graph, we can observe that there is no change in the response of the heterojunction. In the above graph, the difference is due to the contact between FTO and crocodile clips. From the above graph, we can conclude that the heterojunction is stable electrically when exposed to the 60% relative humidity condition.

Figure 4.27

UV Visible Absorption After Different Time Intervals of Exposure to 60% RH.

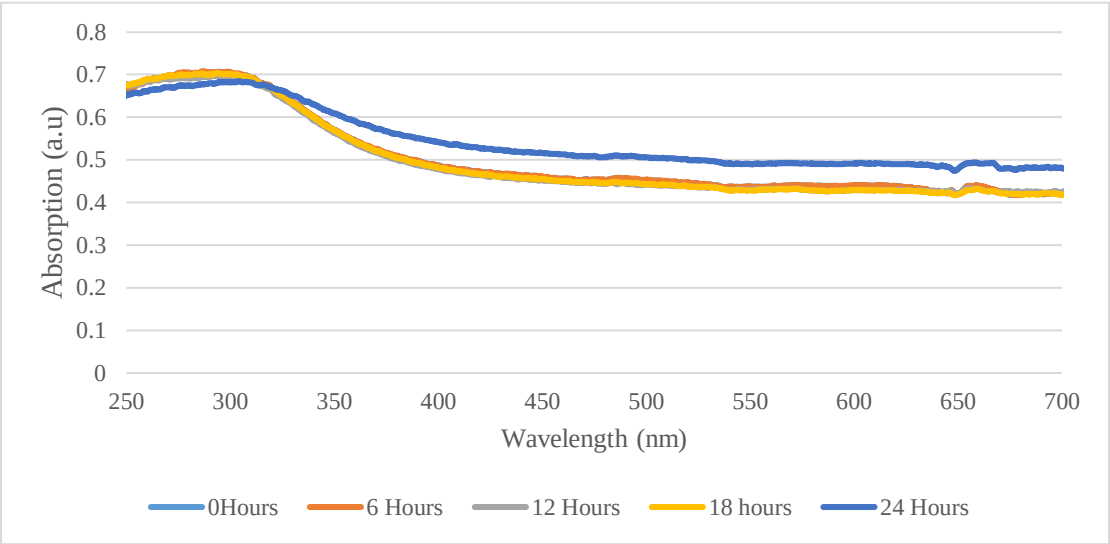

From the above graph, we can say that there is no change in the optical response of the heterojunction. We can conclude that heterojunction is optically stable when exposed to 60 % relative humidity for 24 hours.

4.7 Photocatalysis

We have studied the photocatalytic activity of the above synthesized thin films and heterojunction. The sample is irradiated using a halogen light (projector) calibrated to 1 sun (or) AM1.5 spectrum (1000 W/m^2). We have experimented with UV light exposure as well. We have used a pyranometer and lens on the projector to adjust the incident radiation intensity. Same concentration solutions (10 mg/L) of different dyes were used for comparison. We are only presenting the summarized results, (i.e.) degradation at a specific wavelength for a specific dye. The setup was kept undisturbed and was calibrated after 3-4 cycles. Photocatalytic degradation was analyzed by comparing the absorption peaks from UV-Visible absorption spectroscopy. The change in the absorption values was seen at 470 nm, 522 nm, 661 nm were analyzed for finding the photodegradation rate of Methyl Orange, Methyl Red, and Methylene Blue, respectively. We have kept the photocatalyst sample along with the model dye solution in a beaker in the dark for 2 hours before performing the photocatalytic degradation test. We have found that the absorption value becomes constant after 90-100 minutes (about 1 and a half hours) of dark reaction time. Constant absorption value is a sign for

complete adsorption of the model dye to the surface of the photocatalyst. 2 hours of dark reaction time ensures us that dye is completely absorbed before the exposure to the light and degradation (change in concentration) is solely due to photocatalytic activity. A 10 ml of model dye solution was used for each test and each cycle. Each cycle of a test started with the dark adsorption time as described above and then followed by the exposure to different lighting conditions for 150 minutes (about 2 and a half hours). The change in absorption values was recorded in a regular interval of 15 minutes. We have seen positive values, constant values, negative values in the percentage of change in absorption throughout the experiment. Positive values refer to the decrease of concentration from the first concentration (measured after the 2 hours of dark adsorption) to the concentration after the exposure to the light source for a specific time. Constant values and negative values refer to the no change in the concentration. For all the UV-Vis absorption spectra empty cuvette with DI water was taken as reference. To analyze the results of photocatalytic degradation we have plotted graphically the percentage change in concentration of dye as a function of time. We have used a freshly prepared sample for testing the photocatalytic degradation of each dye.

4.7.1 Photocatalytic Degradation of Methyl Red

Figure 4.28

Photocatalytic Degradation of Methyl Red.

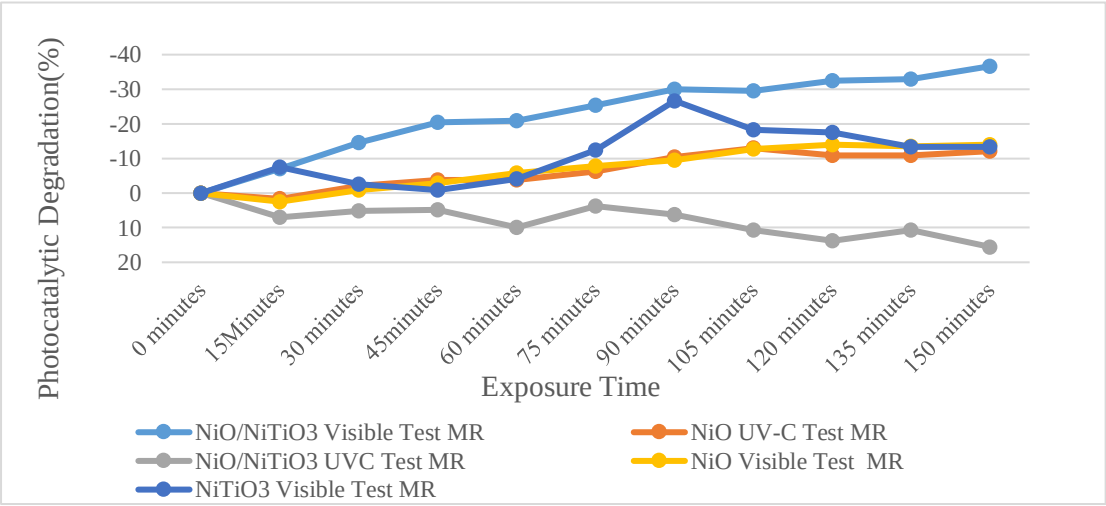

From figure 4.28 we can see that the was no degradation when NiO, $NiTiO_3$, and heterojunction samples were exposed to visible light. Visually the color of the solution

remained unchanged after exposing the sample to visible light for 150 minutes. Similar results were obtained when exposed to UV light. When the heterojunction sample was exposed to UV light, there was 15% of degradation of the methyl red. Visually the solution color changed from red to orange by the end of the experiment. The same was seen in the UV-Visible spectra by reduction of the peak at 522 nm and increase of peak value at 470 nm, over time.

4.7.2 Photocatalytic Degradation of Methyl Orange

Figure 4.29

Photocatalytic Degradation of Methyl Orange

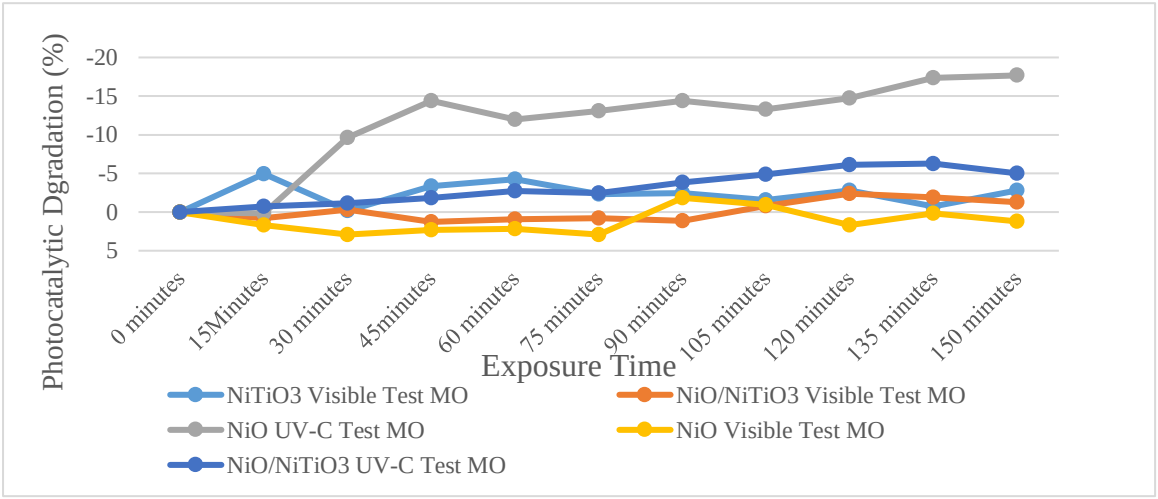

From figure 4.29 we can see that the was no degradation when NiO, $NiTiO_3$, and heterojunction samples were exposed to visible light and UV light. Visually the color of the solution remained unchanged after exposing the sample to visible light(or) UV light for 150 minutes.

4.7.3 Photocatalytic Degradation of Methylene Blue

Figure 4.30

Photocatalytic Degradation of Methylene Blue

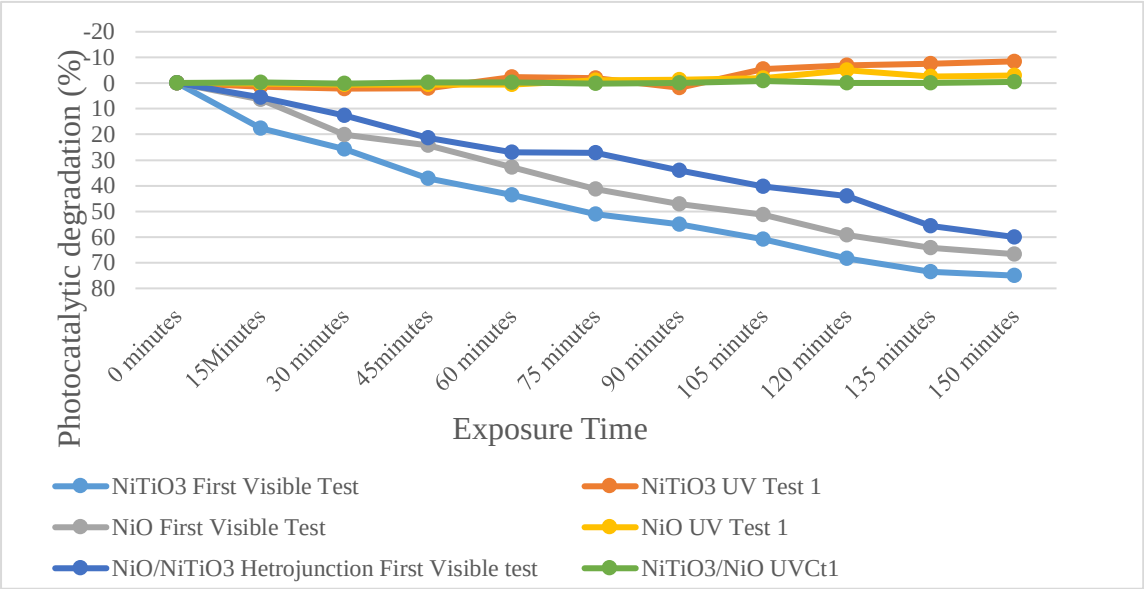

When the samples were illuminated with a visible light source the dye had been showing a significant degradation in the dye concentration, while the samples are illuminated with UV Light (UV, UV -C) the samples were showing no degradation or very little degradation over time. 67% degradation of dye was observed when NiO thin films were exposed to visible light. While there was no degradation observed when NiO thin films were exposed to UV light. 75% degradation was observed when $NiTiO_3$ thin films were exposed to visible light. There was a degradation of 3% when exposed to UV light. 60% degradation of dye was observed when NiO /$NiTiO_3$ Heterojunction was exposed to visible light. There was no degradation observed when NiO /$NiTiO_3$ Heterojunction samples were exposed to UV light.

From all the above results, we were able to notice that all the thin films did not show any degradation in UV-C light and UV light. Only in one case, we have observed degradation of the dye, when we have used Methyl red, and heterojunction was used as a sample under test. From all the above experiments we can conclude that the highest degradation was observed in methylene blue.

An important observation is that there is no enhancement in the photocatalytic degradation efficiency in the case of the heterojunction, which contradicts our primary objective of the study that there would be an enhancement in the photocatalytic degradation efficiency. This could be attributed to the formation of mixed phases of titanates, and non-uniform coating of the titanate thin film. Nickel Titanate thin film showed a better performance when compared to $NiO/NiTiO_3$ heterojunction. This could be attributed to the partial or complete encapsulation of the nickel titanate nanostructures with NiO nanoparticles. There is a possibility of NiO/TiO_2 heterojunctions, which have bands aligned in such a way that it can facilitate photolysis of water instead of photocatalytic degradation. We have observed bubbles on the surface of the sample at the end of the photocatalytic test. (Rawool et al., 2018)

4.8 Repeatability of the Photocatalytic Degradation

From the experiments, we have found that Methylene Blue showed significant degradation when exposed to visible light. To find the repeatability, Photocatalytic degradation experiments were carried out for 2 more cycles with methylene blue as a model dye. Each sample of NiO, $NiTiO_3$, and NiO /$NiTiO_3$ heterojunction was subjected to 3 cycles of photocatalytic degradation tests. After each cycle, the photocatalytic thin films were recovered using 2 different techniques. The first method that was used is the gentle rinsing of the sample with DI water. In the second method, the sample was cleaned with DI water followed by heat treatment (heated at 220°C for 15 minutes) using an oven. The same procedure as the photocatalytic degradation method was used

4.8.1 NiO Thin Film

Figure 4.31

Repeatability of Photocatalytic Degradation of NiO Thin Films

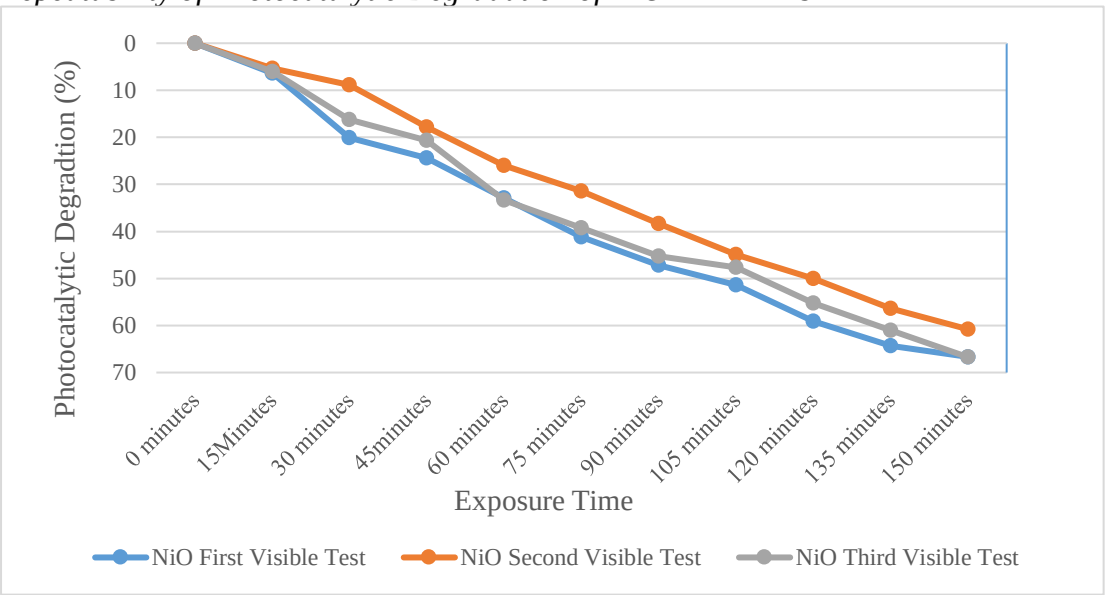

A freshly prepared sample of NiO showed an overall degradation of 67% at the end of 150 minutes. For the second test sample was gently washed with DI water and tested again for photocatalytic degradation. Visually, the sample had a blue color shade on the surface. It has shown a lesser degradation, nearly 61 % of the dye at the end of 150 mins. While for the third test we have heated the ample to 220℃ in a convection oven for 15 mins. Initially, the sample had a blue color tinge on the surface, after heating it had returned to pale brown color. The recovered sample was again tested for its photocatalytic efficiency, and it had given comparable results (67% degradation) to the freshly prepared samples.

4.8.2 $NiTiO_3$ Thin Films

Figure 4.32

Repeatability of Photocatalytic Degradation with $NiTiO_3$ Thin films.

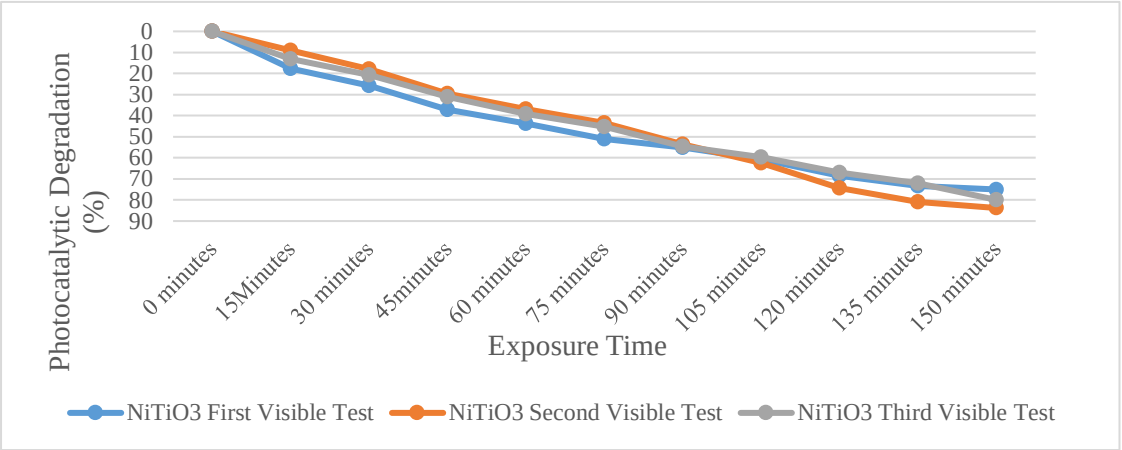

A freshly prepared sample showed an overall degradation of 75% at the end of 150 minutes. While for the second test we have heated the sample to 220℃ in a conventional oven for 15 mins. Initially, the sample had a blue color tinge on the surface, after heating it had returned to yellow color. The recovered sample was again tested for its photocatalytic efficiency, and it had given 83% degradation at the end of 150mins. For the third test sample was gently washed with DI water and tested again for photocatalytic degradation. It has shown a lesser degradation of the dye over time nearly 80 % of the dye at the end of 150 mins.

4.8.3 NiO/NiTiO₃ Heterojunction

Figure 4.33

Repeatability of Photocatalytic Degradation with NiO/NiTiO₃ Heterojunction.

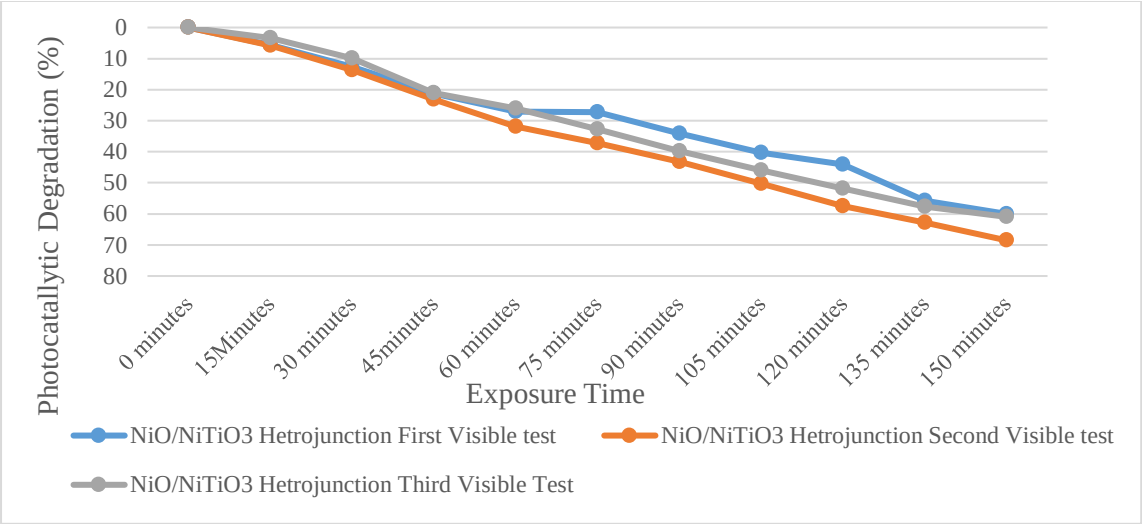

A freshly prepared sample showed an overall degradation of 60% at the end of 150 minutes. While for the second test we have heated the sample to 220℃ in a conventional oven for 15 mins. Initially, the sample had a blue color tinge on the surface, after heating it had returned to dark yellow color. The recovered sample was again tested for its photocatalytic efficiency, and it had given 69% degradation at the end of 150mins. For the third test sample was gently washed with DI water and tested again for photocatalytic degradation. It has shown a lesser degradation of the dye over time nearly 60% of the dye at the end of 150 mins. In all three cases, the degradation rate trend was similar until the end of 1 hour. In cases of 1^{st} and 3^{rd} visible-light photocatalytic degradation tests, they have shown a similar trend until the end of 75 mins.

Some of the common trends that we have seen in all the tests were freshly prepared samples and reheated samples show a similar degradation efficiency at the end of 150 mins when methylene blue was used as a model dye. When methylene blue was used as model dye the degradation of $NiTiO_3$ and $NiO/NiTiO_3$ thin films have shown significant improvement in the degradation efficiency after reheating the samples in the furnace for recovery.

CHAPTER 5
CONCLUSIONS AND FUTURE RECOMMENDATIONS

5.1 Conclusions

We have successfully synthesized the NiO, $NiTiO_3$, and $NiO/NiTiO_3$ heterojunction thin films. All the thin films showed very good stability against high humidity and light conditions. SEM analysis revealed the formation of nanostructured porous thin films with high crystallinity confirmed by using the XRD technique. From the photocatalytic studies, we found nearly 80% degradation in the concentration of the Methylene blue dye after 150 mins of exposure to visible light (A.M 1.5,1000W/m^2). While the heterojunctions and NiO thin films exhibited a similar degradation efficiency. We expect this photocatalytic behavior due to the covering of the $NiTiO_3$ microstructure with NiO nanoparticles all around the surface (observed in the SEM images) and also because of the formation of TiO_2 and NiO phases in $NiTiO_3$. Methylene Blue was the most degraded dye, while methyl orange being the least degradation. The thin films were highly stable concerning optically and electrical properties, even under exposure to visible light and high humid conditions. The synthesis of the pure phase of $NiTiO_3$ thin films is extremely challenging.

5.2 Recommendations for Further Study.

Based on the results obtained in this study, the following recommendations are made for future research:

1) A detailed study on the synthesis techniques to form the heterojunction in a controlled way is required for the robust photocatalyst design.
2) More investigations are required to obtain the pure phase of $NiTiO_3$ thin films to avoid instability in their photocatalytic performances.
3) Detailed photocatalytic studies should be carried out with different kinds of organic pollutants considering other factors, such as light intensity, temperature, and pH to understand the photocatalytic behavior of the heterojunction.

REFERENCES

Akpan, U. G., & Hameed, B. H. (2009). Parameters affecting the photocatalytic degradation of dyes using TiO2-based photocatalysts: A review. In *Journal of Hazardous Materials* (Vol. 170, Issues 2–3, pp. 520–529). Elsevier. https://doi.org/10.1016/j.jhazmat.2009.05.039

Albini, A., & M. F.-C. C., & 2008, undefined. (n.d.). 1908: Giacomo Ciamician and the concept of green chemistry. *Wiley Online Library*. Retrieved July 19, 2020, from https://chemistryeurope.onlinelibrary.wiley.com/doi/abs/10.1002/cssc.20070001

Asahi, R., Morikawa, T., Ohwaki, T., Aoki, K., & Taga, Y. (2001). Visible-light photocatalysis in nitrogen-doped titanium oxides. *Science*, *293*(5528), 269–271. https://doi.org/10.1126/science.1061051

Barhoumi, N., Oturan, N., Olvera-Vargas, H., Brillas, E., Gadri, A., Ammar, S., & Oturan, M. A. (2016). Pyrite as a sustainable catalyst in electro-Fenton process for improving oxidation of sulfamethazine. Kinetics, mechanism and toxicity assessment. *Water Research*, *94*, 52–61. https://doi.org/10.1016/j.watres.2016.02.042

Barrera, L. A., Escobosa, A. C., Nevarez, A., Dominguez, N., Bañuelos, J. L., Westerhoff, P., & Noveron, J. C. (2019). TiO 2 -carbon nanoporous composites prepared via ZnO nanoparticle-templated carbonization of glucose adsorb and photodegrade organic pollutants in water. *Journal of Water Process Engineering*, *28*, 331–338. https://doi.org/10.1016/j.jwpe.2019.02.007

Baur, E., Acta, A. P.-H. C., & 1924, undefined. (n.d.). *The action of light on dissolved silver salts in the presence of zinc oxide*.

Blondeel, G., Harriman, A., materials, D. W.-S. energy, & 1983, undefined. (n.d.). Synergistic effects for the TiO2/RuO2/Pt photodissociation of water. *Elsevier*.

Retrieved July 19, 2020, from https://www.sciencedirect.com/science/article/pii/016516338390045X

Boddy, P. J. (1968). Oxygen Evolution on Semiconducting TiO[sub 2]. *Journal of The Electrochemical Society*, *115*(2), 199. https://doi.org/10.1149/1.2411080

Bruner, L., & Kozak, J. (1911). Zur Kenntnis der Photokatalyse. I. Die Lichtreaktion in Gemischen: Uransalz + Oxalsäure. *Zeitschrift Für Elektrochemie Und Angewandte Physikalische Chemie*, *17*(9), 354–360. https://doi.org/10.1002/bbpc.19110170905

Chaturvedi, V., & Verma, P. (2015). Biodegradation of malachite green by a novel copper-tolerant Ochrobactrum pseudogrignonense strain GGUPV1 isolated from copper mine waste water. *Bioresources and Bioprocessing*, *2*(1). https://doi.org/10.1186/s40643-015-0070-8

Choi, Y. I., Lee, S., Kim, S. K., Kim, Y. il, Cho, D. W., Khan, M. M., & Sohn, Y. (2016). Fabrication of ZnO, ZnS, Ag-ZnS, and Au-ZnS microspheres for photocatalytic activities, CO oxidation and 2-hydroxyterephthalic acid synthesis. *Journal of Alloys and Compounds*, *675*, 46–56. https://doi.org/10.1016/j.jallcom.2016.03.070

Cooper, C. M. (1993). Biological Effects of Agriculturally Derived Surface Water Pollutants on Aquatic Systems—A Review. *Journal of Environmental Quality*, *22*(3), 402–408. https://doi.org/10.2134/jeq1993.00472425002200030003x

Crystallography Open Database: Search results. (n.d.). Retrieved July 9, 2021, from http://www.crystallography.net/cod/result.php

Davidson, D. A., Wilkinson, A. C., Blais, J. M., Kimpe, L. E., McDonald, K. M., & Schindler, D. W. (2003). Orographic Cold-Trapping of Persistent Organic Pollutants by Vegetation in Mountains of Western Canada. *Environmental Science & Technology*, *37*(2), 209–215. https://doi.org/10.1021/es020605q

Eberspacher, C., Fredric, C., Pauls, K., & Serra, J. (2001). Thin-film CIS alloy PV materials fabricated using non-vacuum, particles-based techniques. *Thin Solid Films*, *387*(1–2), 18–22. https://doi.org/10.1016/S0040-6090(00)01729-6

ElSalam, M. (2013). Municipal Solid Waste Management in El-Beheira Governorate, Egypt: a case study in Damanhour City. *Journal of Environmental and Occupational Science*, *2*(3), 131. https://doi.org/10.5455/jeos.20130916100012

Fan, C.-M., Yuan, P.-H., Ding, G.-Y., Wang, Y.-F., & Zhang, X.-C. (2012). Preparation and photocatalytic properties of ilmenite NiTiO 3 powders for degradation of humic acid in water. *International Journal of Minerals, Metallurgy and Materials*, *19*(4). https://doi.org/10.1007/s12613-012-0566-6

Filipovic, L., Selberherr, S., Mutinati, G. C., Brunet, E., Steinhauer, S., Köck, A., Teva, J., Kraft, J., Siegert, J., Schrank, F., Gspan, C., & Grogger, W. (2013). A method for simulating spray pyrolysis deposition in the level set framework. *Engineering Letters*, *21*(4), 224–240. https://graz.pure.elsevier.com/en/publications/a-method-for-simulating-spray-pyrolysis-deposition-in-the-level-s

Fisch, R. (1995). Critical behavior of randomly pinned spin-density waves. *Physical Review B*, *51*(17), 11507–11514. https://doi.org/10.1103/PhysRevB.51.11507

Fouad, O. A., Ismail, A. A., Zaki, Z. I., & Mohamed, R. M. (2006). Zinc oxide thin films prepared by thermal evaporation deposition and its photocatalytic activity. *Applied Catalysis B: Environmental*, *62*(1–2), 144–149. https://doi.org/10.1016/j.apcatb.2005.07.006

Fujishima, A., nature, K. H.-, & 1972, undefined. (n.d.). Electrochemical photolysis of water at a semiconductor electrode. *Nature.Com*. Retrieved July 19, 2020, from https://www.nature.com/articles/238037a0

Gabal, M. A. E. F., al Angari, Y. M., & Obaid, A. Y. (2013). Structural characterization and activation energy of NiTiO3 nanopowders prepared by the co-precipitation and impregnation with calcinations. *Comptes Rendus Chimie*, *16*(8), 704–711. https://doi.org/10.1016/j.crci.2013.01.009

Ge, M., Cao, C., Huang, J., Li, S., Chen, Z., Zhang, K. Q., Al-Deyab, S. S., & Lai, Y. (2016). A review of one-dimensional TiO2 nanostructured materials for environmental and energy applications. In *Journal of Materials Chemistry A* (Vol. 4, Issue 18, pp. 6772–6801). Royal Society of Chemistry. https://doi.org/10.1039/c5ta09323f

Goodeve, C. F., & Kitchener, J. A. (1938). The mechanism of photosensitisation by solids. In *Transactions of the Faraday Society* (Vol. 34, Issue 0, pp. 902–908). The Royal Society of Chemistry. https://doi.org/10.1039/TF9383400902

Gopchandran, K. G., Joseph, B., Abraham, J. T., Koshy, P., & Vaidyan, K. v. (1997). The preparation of transparent electrically conducting indium oxide films by reactive vacuum evaporation. *Vacuum*, *48*(6), 547–550. https://doi.org/10.1016/s0042-207x(97)00023-7

Gunti, S., Kumar, A., & Ram, M. K. (2018). Nanostructured photocatalysis in the visible spectrum for the decontamination of air and water. In *International Materials Reviews* (Vol. 63, Issue 4, pp. 257–282). Taylor and Francis Ltd. https://doi.org/10.1080/09506608.2017.1379264

Halmann, M., Katzir, V., Borgarello, E., Materials, J. K.-S. E., & 1984, undefined. (n.d.). Photoassisted carbon dioxide reduction on aqueous suspensions of titanium dioxide. *Elsevier*. Retrieved July 19, 2020, from https://www.sciencedirect.com/science/article/pii/0165163384900108

Hara, M., Hitoki, G., Takata, T., Kondo, J. N., Kobayashi, H., & Domen, K. (2003). TaON and Ta3N5 as new visible light driven photocatalysts. *Catalysis Today*, *78*(1-4 SPEC.), 555–560. https://doi.org/10.1016/S0920-5861(02)00354-1

Harris, Q. J., Feng, Q., Lee, Y. S., Birgeneau, R. J., & Ito, A. (1997). Random fields and random anisotropies in the mixed ising-XY magnet FexCo1−xTiO3. *Physical Review Letters*, *78*(2), 346–349. https://doi.org/10.1103/PhysRevLett.78.346

Huang, D., Chen, S., Zeng, G., Gong, X., Zhou, C., Cheng, M., Xue, W., Yan, X., & Li, J. (2019). Artificial Z-scheme photocatalytic system: What have been done and where to go? In *Coordination Chemistry Reviews* (Vol. 385, pp. 44–80). Elsevier B.V. https://doi.org/10.1016/j.ccr.2018.12.013

Hyun, J. K., Zhang, S., & Lauhon, L. J. (2013). Nanowire Heterostructures. *Annual Review of Materials Research*, *43*(1), 451–479. https://doi.org/10.1146/annurev-matsci-071312-121659

Inceesungvorn, B., Teeranunpong, T., Nunkaew, J., Suntalelat, S., & Tantraviwat, D. (2014). Novel NiTiO3/Ag3VO4 composite with enhanced photocatalytic performance under visible light. *Catalysis Communications*, *54*, 35–38. https://doi.org/10.1016/j.catcom.2014.05.015

Inoue, T., Fujishima, A., Konishi, S., Nature, K. H.-, & 1979, undefined. (n.d.). Photoelectrocatalytic reduction of carbon dioxide in aqueous suspensions of semiconductor powders. *Nature.Com*. Retrieved July 19, 2020, from https://www.nature.com/articles/277637a0

Jiang, L., Yuan, X., Zeng, G., Liang, J., Wu, Z., & Wang, H. (2018). Construction of an all-solid-state Z-scheme photocatalyst based on graphite carbon nitride and its enhancement to catalytic activity. In *Environmental Science: Nano* (Vol. 5, Issue 3, pp. 599–615). Royal Society of Chemistry. https://doi.org/10.1039/c7en01031a

Jiang, Q., Ji, C., Riley, D., & Xie, F. (2018). Boosting the Efficiency of Photoelectrolysis by the Addition of Non-Noble Plasmonic Metals: Al & Cu. *Nanomaterials*, *9*(1), 1. https://doi.org/10.3390/nano9010001

Jiang, Z., Zhu, C., Wan, W., Qian, K., & Xie, J. (2016). Constructing graphite-like carbon nitride modified hierarchical yolk-shell TiO2 spheres for water pollution treatment and hydrogen production. *Journal of Materials Chemistry A*, *4*(5), 1806–1818. https://doi.org/10.1039/c5ta09919f

Joseph, B., Gopchandran, K. G., Manoj, P. K., Koshy, P., & Vaidyan, V. K. (1999). Optical and electrical properties of zinc oxide films prepared by spray pyrolysis. In *Bull. Mater. Sci* (Vol. 22, Issue 5). https://link.springer.com/content/pdf/10.1007/BF02745554.pdf

Kampa, M., & Castanas, E. (2008). Human health effects of air pollution. In *Environmental Pollution* (Vol. 151, Issue 2, pp. 362–367). https://doi.org/10.1016/j.envpol.2007.06.012

Khan, M. M., Adil, S. F., & Al-Mayouf, A. (2015). Metal oxides as photocatalysts. In *Journal of Saudi Chemical Society* (Vol. 19, Issue 5, pp. 462–464). Elsevier. https://doi.org/10.1016/j.jscs.2015.04.003

Khan, M. M., Ansari, S. A., Pradhan, D., Han, D. H., Lee, J., & Cho, M. H. (2014). Defect-induced band gap narrowed CeO2 nanostructures for visible light activities. *Industrial and Engineering Chemistry Research*, *53*(23), 9754–9763. https://doi.org/10.1021/ie500986n

Kumar Ray, S., Dhakal, D., Gyawali, G., Joshi, B., Raj Koirala, A., & Wohn Lee, S. (2019). Transformation of tetracycline in water during degradation by visible light driven Ag nanoparticles decorated A-NiMoO4 nanorods: Mechanism and pathways. *Chemical Engineering Journal*, *373*, 259–274. https://doi.org/10.1016/j.cej.2019.05.041

Kumar, S., Science, K. R.-A. S., & 2017, undefined. (n.d.). Comparison of modification strategies towards enhanced charge carrier separation and photocatalytic degradation activity of metal oxide semiconductors. *Elsevier*. Retrieved July 20, 2020, from https://www.sciencedirect.com/science/article/pii/S0169433216315173

Lei, Z., You, W., Liu, M., Zhou, G., Takata, T., Hara, M., Domen, K., & Li, C. (2003). Photocatalytic water reduction under visible light on a novel ZnIn2S4 catalyst synthesized by hydrothermal method. *Chemical Communications*, *3*(17), 2142–2143. https://doi.org/10.1039/b306813g

Lenin, N., Karthik, A., Sridharpanday, M., … M. S.-J. of M., & 2016, undefined. (n.d.). Electrical and magnetic behavior of iron doped nickel titanate (Fe3+/NiTiO3) magnetic nanoparticles. *Elsevier*. Retrieved July 20, 2020, from https://www.sciencedirect.com/science/article/pii/S0304885315305394

Li, Q., Li, X., Wageh, S., Al-Ghamdi, A. A., & Yu, J. (2015). CdS/Graphene Nanocomposite Photocatalysts. *Advanced Energy Materials*, *5*(14). https://doi.org/10.1002/aenm.201500010

Li, S., Hu, S., Jiang, W., Liu, Y., Zhou, Y., Liu, Y., & Mo, L. (2018). Hierarchical architectures of bismuth molybdate nanosheets onto nickel titanate nanofibers: Facile synthesis and efficient photocatalytic removal of tetracycline hydrochloride. *Journal of Colloid and Interface Science*, *521*, 42–49. https://doi.org/10.1016/j.jcis.2018.03.033

Lin, Y. J., Chang, Y. H., Yang, W. D., & Tsai, B. S. (2006a). Synthesis and characterization of ilmenite NiTiO3 and CoTiO3 prepared by a modified Pechini method. *Journal of Non-Crystalline Solids*, *352*(8), 789–794. https://doi.org/10.1016/j.jnoncrysol.2006.02.001

Lin, Y. J., Chang, Y. H., Yang, W. D., & Tsai, B. S. (2006b). Synthesis and characterization of ilmenite NiTiO3 and CoTiO3 prepared by a modified Pechini method. *Journal of Non-Crystalline Solids*, *352*(8), 789–794. https://doi.org/10.1016/J.JNONCRYSOL.2006.02.001

Lopes, K. P., Cavalcante, L. S., Simões, A. Z., Varela, J. A., Longo, E., & Leite, E. R. (2009). NiTiO3 powders obtained by polymeric precursor method: Synthesis and characterization. *Journal of Alloys and Compounds*, *468*(1–2), 327–332. https://doi.org/10.1016/j.jallcom.2007.12.085

Lu, D., Wang, H., Zhao, X., Kondamareddy, K. K., Ding, J., Li, C., & Fang, P. (2017). Highly efficient visible-light-induced photoactivity of Z-scheme g-C3N4/Ag/MoS2 ternary photocatalysts for organic pollutant degradation and production of hydrogen. *ACS Sustainable Chemistry and Engineering*, *5*(2), 1436–1445. https://doi.org/10.1021/acssuschemeng.6b02010

Mahmoud, S. A., Shereen, A., & Tarawnh, M. A. (2011). Structural and Optical Dispersion Characterisation of Sprayed Nickel Oxide Thin Films. *Journal of Modern Physics*, *02*(10), 1178–1186. https://doi.org/10.4236/jmp.2011.210147

Manifacier, J. C., Fillard, J. P., & Bind, J. M. (1981). Deposition of In2O3SnO2 layers on glass substrates using a spraying method. *Thin Solid Films*, *77*(1–3), 67–80. https://doi.org/10.1016/0040-6090(81)90361-8

Marschall, R. (2014). Photocatalysis: Semiconductor Composites: Strategies for Enhancing Charge Carrier Separation to Improve Photocatalytic Activity (Adv. Funct. Mater. 17/2014). *Advanced Functional Materials*, *24*(17), 2420–2420. https://doi.org/10.1002/adfm.201470108

Moniz, S. J. A., Shevlin, S. A., Martin, D. J., Guo, Z.-X., & Tang, J. (n.d.). Visible-Light Driven Heterojunction Photocatalysts for Water Splitting-A Critical Review. In *pubs.rsc.org*. Retrieved July 19, 2020, from https://pubs.rsc.org/lv/content/articlehtml/2015/ee/c4ee03271c

Nguyen-Phan, T.-D., Huy, C. N., Kim, C.-K., & Shin, E. W. (2013). Facile microwave-assisted synthesis and controllable architecture of three-dimensional nickel titanate †. *J. Name*, *00*, 1–3. https://doi.org/10.1039/x0xx00000x

Niedermayer, S., Fürhapper, C., Nagl, S., Polleres, S., & Schober, K. P. (2013). VOC sorption and diffusion behavior of building materials. *European Journal of Wood and Wood Products*, *71*(5), 563–571. https://doi.org/10.1007/s00107-013-0713-4 *OEHHA. California office of environmental health hazard assessment. 2007*

Peng, Y., Yan, M., Chen, Q. G., Fan, C. M., Zhou, H. Y., & Xu, A. W. (2014). Novel one-dimensional Bi2O3-Bi2WO 6 p-n hierarchical heterojunction with enhanced photocatalytic activity. *Journal of Materials Chemistry A*, *2*(22), 8517–8524. https://doi.org/10.1039/c4ta00274a

Pham, T., Kang, S., Science, E. S.-A. S., & 2017, undefined. (n.d.). Optical and structural properties of Mo-doped NiTiO3 materials synthesized via modified Pechini methods. *Elsevier*. Retrieved July 20, 2020, from https://www.sciencedirect.com/science/article/pii/S0169433217307821

Pham, T., Nguyen-Huy, C., Letters, E. S.-M., & 2016, undefined. (n.d.). NiTiO3/reduced graphene oxide materials synthesized by a two-step microwave-assisted method. *Elsevier*. Retrieved July 20, 2020, from https://www.sciencedirect.com/science/article/pii/S0167577X16312459

Phani, A. R., & Santucci, S. (2001). Structural characterization of nickel titanium oxide synthesized by sol-gel spin coating technique. *Thin Solid Films*, *396*(1–2), 1–4. https://doi.org/10.1016/S0040-6090(01)01131-2

Pimentel D, McLaughlin L, Zepp A, et al. Environmental and economic effects of reducing pesticide use. BioSci. 1991;41(6):402–409.

Puddu, V., Mokaya, R., & Li Puma, G. (2007). Novel one step hydrothermal synthesis of TiO2/WO3 nanocomposites with enhanced photocatalytic activity. *Chemical Communications*, *45*, 4749–4751. https://doi.org/10.1039/b711559h

Qu, Y., Zhou, W., Ren, Z., Du, S., Meng, X., Tian, G., Pan, K., Wang, G., & Fu, H. (2012). Facile preparation of porous NiTiO 3 nanorods with enhanced visible-light-driven photocatalytic performance. *Journal of Materials Chemistry*, *22*(32), 16471–16476. https://doi.org/10.1039/C2JM32044D

Qu, Z., Rong, Y., Tang, L., Shu, X., Liu, X., Zhang, Z., & Wang, J. (2017). A new visible-light-induced Z-scheme photocatalytic system: Er3+:Y3Al5O12/(MoS2/NiGa2O4)-(BiVO4/PdS) for refractory pollutant degradation with simultaneous hydrogen evolution. *Molecular Catalysis*, *441*, 10–20. https://doi.org/10.1016/j.mcat.2017.08.001

Rawool, S. A., Pai, M. R., Banerjee, A. M., Arya, A., Ningthoujam, R. S., Tewari, R., Rao, R., Chalke, B., Ayyub, P., Tripathi, A. K., & Bharadwaj, S. R. (2018). pn Heterojunctions in NiO:TiO2 composites with type-II band alignment assisting sunlight driven photocatalytic H2 generation. *Applied Catalysis B: Environmental*, *221*, 443–458. https://doi.org/10.1016/J.APCATB.2017.09.004

Reid, W. D., Ilett, K. F., Glick, J. M., & Krishna, G. (1973). Metabolism and binding of aromatic hydrocarbons in the lung. Relationship to experimental bronchiolar necrosis. *AMER.REV.RESP.DIS.*, *107*(4), 539–551. https://doi.org/10.1164/arrd.1973.107.4.539

Robinson, T., McMullan, G., Marchant, R., & Nigam, P. (2001). Remediation of dyes in textile effluent: A critical review on current treatment technologies with a proposed alternative. *Bioresource Technology*, *77*(3), 247–255. https://doi.org/10.1016/S0960-8524(00)00080-8

Romero, R., Martin, F., Ramos-Barrado, J. R., & Leinen, D. (2010). Synthesis and characterization of nanostructured nickel oxide thin films prepared with chemical spray pyrolysis. *Thin Solid Films*, *518*(16), 4499–4502. https://doi.org/10.1016/j.tsf.2009.12.016

Ruan, L., Wang, X., Wang, T., Ren, Z., Chen, Y., Zhao, R., Zhou, D., Fu, G., Li, S., Gao, L., Lu, Y., Wang, Z., Tian, H., Kong, X., & Han, G. (2019). Surface Defect-Controlled Growth and High Photocatalytic H2 Production Efficiency of Anatase TiO2 Nanosheets. *ACS Applied Materials and Interfaces*, *11*(40), 37256–37262. https://doi.org/10.1021/acsami.9b11233

Sadjadi, M. S., Zare, K., Khanahmadzadeh, S., & Enhessari, M. (2008). Structural characterization of NiTiO3 nanopowders prepared by stearic acid gel method. *Materials Letters*, *62*(21–22), 3679–3681. https://doi.org/10.1016/j.matlet.2008.04.028

Saito, K., Komiya, Y., Sohmiya, M., Ogasawara, M., & Kato, S. (2020). *Journal of Asian Ceramic Societies ISSN: (Print) (Online) Journal homepage: https://www.tandfonline.com/loi/tace20 A phase separation in a protonated layered nickel titanate to form Ni-doped anatase/rutile TiO 2 nanocomposite with efficient visible-light responsive photocatalytic activity*. https://doi.org/10.1080/21870764.2020.1793875

Sakhare, Y. S., Thakare, N. R., & Ubale, A. U. (2016). Influence of quantity of spray solution on the physical properties of spray-deposited nanocrystalline MgSe thin films. *St. Petersburg State Polytechnical University Journal. Physics and Mathematics*, *237*(1), 29–40. https://doi.org/10.5862/jpm.237.3

Salthammer, T. (2016). Very volatile organic compounds: An understudied class of indoor air pollutants. *Indoor Air*, *26*(1), 25–38. https://doi.org/10.1111/ina.12173

Saravanan, R., Gupta, V. K., Narayanan, V., & Stephen, A. (2013). Comparative study on photocatalytic activity of ZnO prepared by different methods. *Journal*

of Molecular Liquids, *181*, 133–141. https://doi.org/10.1016/j.molliq.2013.02.023

Sasi, B., Gopchandran, K., Manoj, P., Koshy, P., Vacuum, P. R.-, & 2002, undefined. (n.d.). Preparation of transparent and semiconducting NiO films. *Elsevier*. Retrieved July 20, 2020, from https://www.sciencedirect.com/science/article/pii/S0042207X02002993

Sato, H., Minami, T., Takata, S., & Yamada, T. (1993). Transparent conducting p-type NiO thin films prepared by magnetron sputtering. *Thin Solid Films*, *236*(1–2), 27–31. https://doi.org/10.1016/0040-6090(93)90636-4

Sawatzky, G. A., & Allen, J. W. (1984). Magnitude and origin of the band gap in NiO. *Physical Review Letters*, *53*(24), 2339–2342. https://doi.org/10.1103/PhysRevLett.53.2339

Schneider, J., Matsuoka, M., Takeuchi, M., Zhang, J., Horiuchi, Y., Anpo, M., & Bahnemann, D. W. (2014). Understanding TiO2photocatalysis: Mechanisms and materials. In *Chemical Reviews* (Vol. 114, Issue 19, pp. 9919–9986). American Chemical Society. https://doi.org/10.1021/cr5001892

Shi, W., & Chopra, N. (2013). Nanoscale heterostructures for photoelectrochemical water splitting and photodegradation of pollutants. *Nanomaterials and Energy*, *2*(3), 158–178. https://doi.org/10.1680/nme.13.00009

Taguchi, H., Matsuda, D., Nagao, M., Tanihata, K., & Miyamoto, Y. (1992). Synthesis of Perovskite-Type (La1−xSrx)MnO3 (O X 0.3) at Low Temperature. *Journal of the American Ceramic Society*, *75*(1), 201–202. https://doi.org/10.1111/j.1151-2916.1992.tb05465.x

Thomassen, L. (2002). An X-Ray Investigation of the System Cr2O3-NiO1. *Journal of the American Chemical Society*, *62*(5), 1134–1136. https://doi.org/10.1021/JA01862A037

Vijayalakshmi, R., & Rajendran, V. (2012). Effect of reaction temperature on size and optical properties of NiTiO 3 nanoparticles. *E-Journal of Chemistry*, *9*(1), 282–288. https://doi.org/10.1155/2012/607289

Wang, H., Yuan, X., Wang, H., Chen, X., Wu, Z., Jiang, L., Xiong, W., Zhang, Y., & Zeng, G. (n.d.). One-step calcination method for synthesis of mesoporous g-C 3 N 4 /NiTiO 3 heterostructure photocatalyst with improved visible light photoactivity. In *pubs.rsc.org*. Retrieved July 20, 2020, from https://pubs.rsc.org/ko/content/articlehtml/2015/ra/c5ra18117h

Wang, H., Zhang, L., Chen, Z., Hu, J., Li, S., … Z. W.-C. S., & 2014, undefined. (n.d.). Semiconductor heterojunction photocatalysts: design, construction, and photocatalytic performances. *Pubs.Rsc.Org*. Retrieved July 19, 2020, from https://pubs.rsc.org/ko/content/articlehtml/2014/cs/c4cs00126e

Wang, J. L., Li, Y. Q., Byon, Y. J., Mei, S. G., & Zhang, G. L. (2013). Synthesis and characterization of NiTiO3 yellow nano pigment with high solar radiation reflection efficiency. *Powder Technology*, *235*, 303–306. https://doi.org/10.1016/j.powtec.2012.10.044

Wang, Y., Suzuki, H., Xie, J., Tomita, O., Martin, D. J., Higashi, M., Kong, D., Abe, R., & Tang, J. (2018). Mimicking Natural Photosynthesis: Solar to Renewable H2 Fuel Synthesis by Z-Scheme Water Splitting Systems. In *Chemical Reviews* (Vol. 118, Issue 10, pp. 5201–5241). American Chemical Society. https://doi.org/10.1021/acs.chemrev.7b00286

Wania, F., & MacKay, D. (1996). Wania F 1996 EST,30,9,390A.pdf. *Environmental Science & Technology*, *30*(9), 390A-396A. https://doi.org/10.1021/es962399q

WHO. WHO guidelines for indoor air quality: selected pollutants, W. H. Organiazation, Editor. 2010: Europe.

Xie, S., Zhang, Q., Liu, G., & Wang, Y. (2015). Photocatalytic and Photoelectrocatalytic Reduction of CO2 Using Heterogeneous Catalysts with Controlled Nanostructures Photocatalytic and photoelectrocatalytic reduction of CO 2 using heterogeneous catalysts with controlled nanostructures. *Chem. Commun*, *52*, 35. https://doi.org/10.1039/c5cc07613g

Yang, B., Bai, X., Wang, J., Fang, M., Wu, X., Liu, Y., Huang, Z., Lao, C.-Y., & Min, X. (2019). Photocatalytic Performance of NiO/NiTiO3 Composite Nanofiber Films. *Catalysts 2019, Vol. 9, Page 561*, *9*(6), 561. https://doi.org/10.3390/CATAL9060561

Yang, Q., Huang, J., Zhong, J., Chen, J., Li, J., & Sun, S. (2017). Charge separation behaviors of novel AgI/BiOI heterostructures with enhanced solar-photocatalytic performance. *Current Applied Physics*, *17*(9), 1202–1207. https://doi.org/10.1016/j.cap.2017.05.016

Yu, J., & Yu, X. (2008). Hydrothermal synthesis and photocatalytic activity of zinc oxide hollow spheres. *Environmental Science and Technology*, *42*(13), 4902–4907. https://doi.org/10.1021/es800036n

Zhang, P., Wang, T., Chang, X., & Gong, J. (2016). Effective Charge Carrier Utilization in Photocatalytic Conversions. *Accounts of Chemical Research*, *49*(5), 911–921. https://doi.org/10.1021/acs.accounts.6b00036

Zhang, Z., Shao, C., Li, X., Zhang, L., Xue, H., Wang, C., & Liu, Y. (2010). Electrospun nanofibers of ZnO-SnO2 heterojunction with high photocatalytic activity. *Journal of Physical Chemistry C*, *114*(17), 7920–7925. https://doi.org/10.1021/jp100262q

Zhao, P., Gong, W., Mao, G., Li, J., Xu, F., & Shi, J. (2016). Pollution of HCHs, DDTs and PCBs in tidal flat of Hangzhou Bay 2009–2013. *Chinese Journal of*

Oceanology and Limnology, *34*(3), 539–548. https://doi.org/10.1007/s00343-016-4384-y

Zhou, H., Qu, Y., Zeid, T., & Duan, X. (2012). Towards highly efficient photocatalysts using semiconductor nanoarchitectures. In *Energy and Environmental Science* (Vol. 5, Issue 5, pp. 6732–6743). The Royal Society of Chemistry. https://doi.org/10.1039/c2ee03447f

Zhu, S., & Wang, D. (2017). Photocatalysis: Basic principles, diverse forms of implementations and emerging scientific opportunities. In *Advanced Energy Materials* (Vol. 7, Issue 23). Wiley-VCH Verlag. https://doi.org/10.1002/aenm.201700841

VITA

Sai Aditya Vullikanti is a strong believer in creating a world that is a more sustainable, inclusive, and global world. He believes that every young individual given a chance can create a change in the world. He has experience working with Startups, Government Organizations, Corporate companies and was actively involved in the research and development of innovative and impactful products in the organizations. He has completed his bachelor's degree in the field of Electronics and Communication engineering from Jawaharlal Nehru Technological University Hyderabad. He has worked in the sectors of IoT, Wearables, System Architect Design before his masters at AIT.

His areas of research and interest include smart sensors, photovoltaics, energy storage devices, embedded systems, optoelectronics applications. This work was done as a part of thesis submission, where he has applied the skills and knowledge obtained from the Center of Excellence in Nanotechnology during his course work at AIT. Other areas of interest include Fine Art, Impact Entrepreneurship, Embedded Systems. Apart from the academics, he has been volunteering in creating of impact entrepreneurial mindset in the community of AIT by involving and partnering with international organizations like United Nations, Hult Prize Foundation. He has also represented AIT in many international avenues across the world. With the completion of this study, he has completed his master's degree in the field of Nanotechnology, from Centre of Excellence in Nanotechnology, AIT. He wishes to use his knowledge and experience to build a better world, by innovating and creating solutions that can create positive impact in lives of many people across the world.